Volume 49
Number 3
7 February 2020
Pages 647–1034

Chem Soc Rev

Chemical Society Reviews

rsc.li/chem-soc-rev

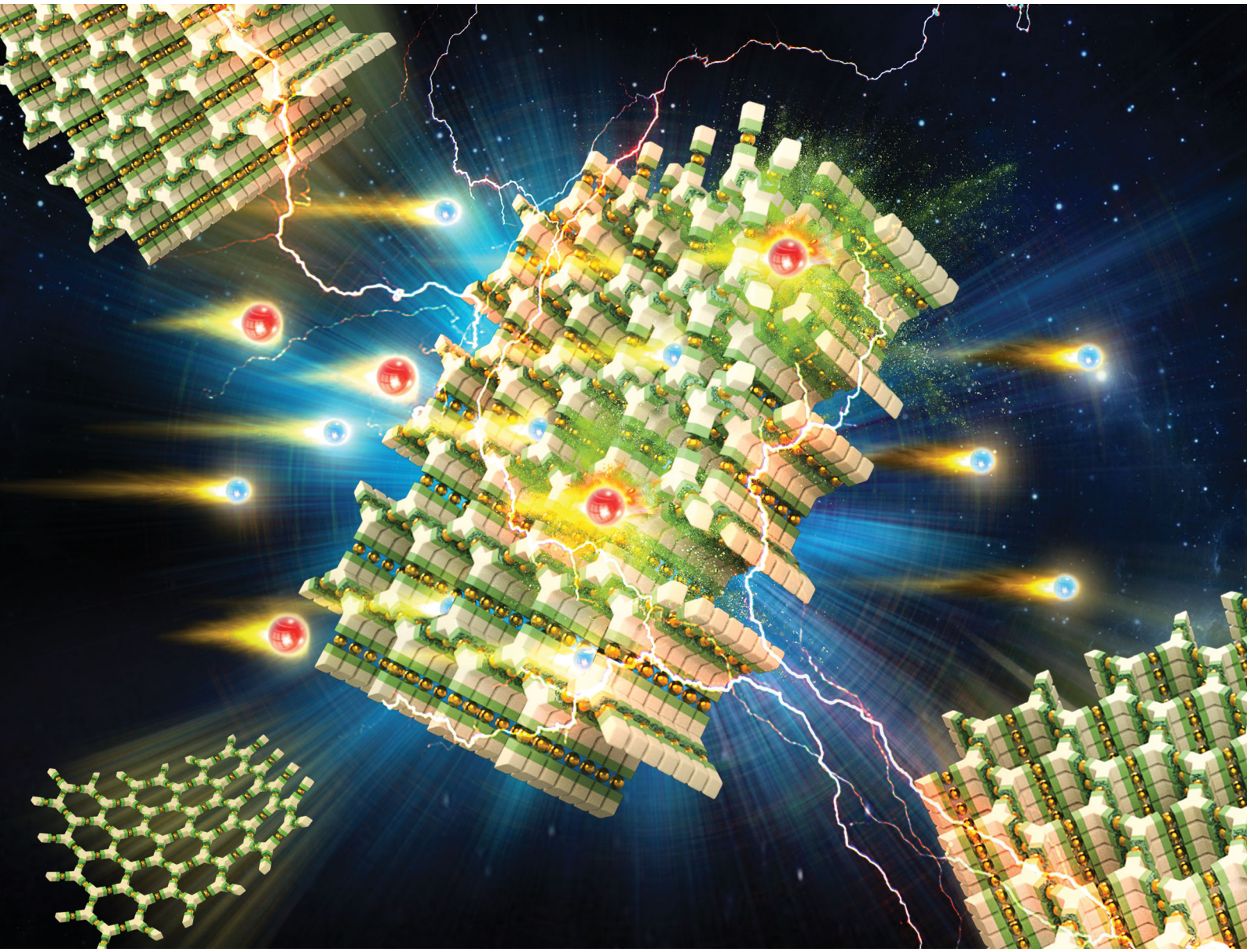

ISSN 0306-0012

ROYAL SOCIETY OF CHEMISTRY

REVIEW ARTICLE

Yao Chen, Zhenjie Zhang, Shengqian Ma *et al.*

Covalent organic frameworks for separation applications

Chem Soc Rev

REVIEW ARTICLE

View Article Online
View Journal | View Issue

Cite this: *Chem. Soc. Rev.*, 2020, **49**, 708

Covalent organic frameworks for separation applications

Zhifang Wang,†[ae] Sainan Zhang,†[a] Yao Chen,*[abc] Zhenjie Zhang*[ae] and Shengqian Ma*[d]

Covalent organic frameworks (COFs) are an emerging class of crystalline porous polymers with highly tuneable structures and functionalities. COFs have been proposed as ideal materials for applications in the energy-intensive field of molecular separation due to their notable intrinsic features such as low density, exceptional stability, high surface area, and readily adjustable pore size and chemical environment. This review attempts to highlight the key advancements made in the synthesis of COFs for diverse separation applications such as water treatment or the separation of gas mixtures and organic molecules, including chiral and isomeric compounds. Methods proposed for the fabrication of COF-based columns and continuous membranes for practical applications are also discussed in detail. Finally, a perspective regarding the remaining challenges and future directions for COF research in the field of separation has also been presented.

Received 30th November 2019

DOI: 10.1039/c9cs00827f

rsc.li/chem-soc-rev

[a] *State Key Laboratory of Medicinal Chemical Biology, College of Chemistry, Nankai University, Tianjin 300071, People's Republic of China. E-mail: zhangzhenjie@nankai.edu.cn, chenyao@nankai.edu.cn*
[b] *College of Pharmacy, Nankai University, Tianjin 300071, People's Republic of China*
[c] *National Institute for Advanced Materials, Nankai University, Tianjin 300071, People's Republic of China*
[d] *Department of Chemistry, University of South Florida, 4202 East Fowler Avenue, Tampa, Florida 33620, USA. E-mail: sqma@usf.edu*
[e] *Key Laboratory of Advanced Energy Materials Chemistry (Ministry of Education), Renewable Energy Conversion and Storage Center, Nankai University, Tianjin 300071, People's Republic of China*
† These authors contributed equally to this work.

1. Introduction

Separation processes play an integral role in industry and our daily life, involving processes such as distillation, crystallization, concentration, and purification.[1–7] However, these traditional separation technologies are typically accompanied by high energy consumption. For example, distillation alone accounted for 10–15% of the world's total energy consumption in 2016 making it one of the biggest contributing factors to global environmental issues such as climate change.[8] Therefore, developing alternative separation techniques with low energy consumption would decrease the global energy demand, with

Zhifang Wang

Dr Zhifang Wang received his BSc degree from HuaiBei Normal University in 2013. In 2016, he obtained his MS degree from Tianjin University (advisor: Professor Bin Zhang). In 2019, he obtained his PhD degree from Nankai University (advisor: Professor Zhenjie Zhang) and then continued his postdoctoral research in the Zhang group. His research focuses on the design, synthesis, and application of organic porous materials including covalent organic frameworks (COFs) and porous organic cages (POCs).

Sainan Zhang

Dr Sainan Zhang received her PhD degree in Chemical Biology from Nankai University in 2019 from Professor Yao Chen's group. She is now continuing her post-doctoral research in Chen's group at Nankai University. She received the first batch of special grants from the China Postdoctoral Science Foundation. Her current research interests focus on the use of porous framework materials for value-added applications such as chiral recognition and separation.

subsequent benefits to the environment. Adsorption-based and membrane-based technologies have attracted increasing attention and demonstrated great potential in industrial processes due to their advantages such as high efficiency, easy operation, low energy consumption and environmental sustainability.[9–12] The separation media for adsorption-based and membrane-based technologies were previously consisted of conventional porous materials including activated carbon,[13,14] zeolites,[15,16] hyper-cross-linked polymers (HCPs),[17,18] conjugated microporous polymers (CMPs),[19–21] porous organic polymers (POPs)[22,23] and metal–organic frameworks (MOFs).[24–28] Among them, crystalline materials, especially MOFs and zeolites, often show superior separation performance over amorphous materials (*e.g.* activated carbon and PAFs) due to their ordered structures, tunable pore size, high surface areas, *etc.*[29–36] For instance, MOFs have created many benchmarks for hydrocarbon separations among all porous materials.[37–42] Recently, covalent organic frameworks (COFs) have emerged as a new generation of crystalline framework materials,[43–48] which can be considered as a sister material to MOFs,[49–53] constructed from pure organic building blocks using the design principles of 'reticular chemistry'.[54–59] However, using COFs as the separation media is still relatively understudied compared with MOFs due to their synthetic challenges and comparatively low crystallinity.[60–62]

Since the pioneering work of Yaghi and co-workers in 2005,[63] a great variety of COFs have been reported, including boroxine-linked,[64] boronate ester-linked,[65] imine-linked,[52,66] hydrazone-linked,[67] azine-linked,[68] β-ketoenamine-linked,[69,70] triazine-linked,[71,72] imide-linked,[73] phenazine-linked,[74] and sp^2-carbon linked COFs[75,76] (Fig. 1). Their well-defined crystalline structures, low density, good chemical stability, large surface area, and facilely-tailored functionalities have endowed COF materials with unique properties and great potential in diverse applications, such as catalysis,[77–80] gas adsorption,[81] separation,[82] drug delivery,[83,84] functional devices[85] and supercapacitors.[86,87] Among them, the separation application of COFs is attracting particular attention due to the distinct structural features of COFs (*e.g.* ordered pore channels, uniform pore size) and facile membrane formation.[60–62] Generally, COF-based separation methodologies can be divided into two categories: packed bed separation (adsorption-based) and membrane-based separation. In packed bed separation, a multi-component mixture passes through fixed-bed adsorbers or a column packed with adsorbents to afford a single-component product based on the differences in adsorption capability among components towards the adsorbent. For membrane separation, COF membranes can separate the mixtures based on differences in the diffusion rates between each component, or based on molecular sieving effects between the mixture and the COF materials. Over the past decade, COFs have been reported for various separation applications including methane purification,[88]

Yao Chen

Dr Yao Chen obtained her master's degree from Nanjing Tech University, and then obtained her PhD degree from the University of South Florida. After finishing a postdoctoral training at UC San Diego, she moved back to China, and is now a full professor of the State Key Laboratory of Medicinal Chemical Biology and College of Pharmacy at Nankai University. Her current research interest focuses on the construction of biomolecule-incorporated composite materials with various functionalities, and their biological and medicinal related applications, such as biocatalysis, chiral separation and medicinal applications.

Zhenjie Zhang

Dr Zhenjie Zhang (Nankai University, China) earned his BSc and MS degrees from Nankai University. In 2014, he obtained his PhD degree from the University of South Florida in the field of metal–organic frameworks. He did his postdoctoral research with Professor Seth M. Cohen at UC San Diego (2014–2016) before embarking on his independent career as a full professor of Inorganic Chemistry at Nankai University. The Zhang group is currently focusing on developing new crystalline materials (e.g. MOFs, COFs, MOPs) for value-added product purification (e.g. light hydrocarbon separation), membrane fabrication as well as fabricating smart actuators or robots.

Shengqian Ma

Dr Shengqian Ma obtained his BS degree from Jilin University (China) in 2003, and graduated from Miami University (Ohio) with a PhD degree in 2008. After a two-year Director's Postdoctoral Fellowship at Argonne National Laboratory, he joined the Department of Chemistry at the University of South Florida (USF) as an Assistant Professor in August 2010. He was promoted to an Associate Professor with early tenure in 2015 and to a Full Professor in 2018. His current research interest focuses on task-specific design and functionalization of advanced porous materials for energy, biological, and environmental-related applications.

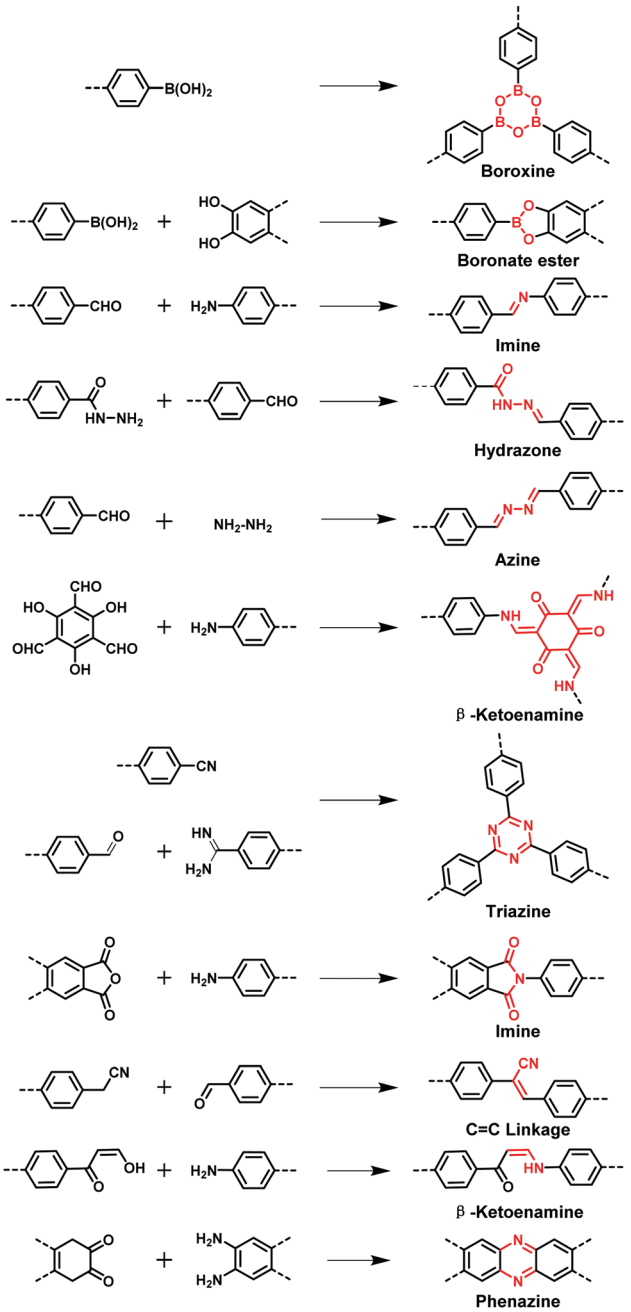

Fig. 1 The classic reactions used for the construction of COFs.

separation of hydrogen isotopes,[89] carbon dioxide/nitrogen separation,[90] hydrogen purification,[91] homologue separation,[92] water treatment,[93] chiral separation,[94] organic molecule separation,[95] and removing acetylene from ethylene (Fig. 2).[96] This review will give a comprehensive survey on current research progress regarding the separation applications of COFs, which covers packed bed systems for adsorption-based separations and membrane-based separations. The state-of-the-art and strategies used for COF-based separation applications have been summarized, as well as a perspective of the existing challenges and future directions for COF research in separation is provided.

2. Strategies to utilize COFs for separation application

There are three different mechanisms predominantly involved in the transport of mixtures across porous materials: separation due to thermodynamic equilibrium arising because of differing adsorbate–adsorbent interactions, kinetic separation due to differing diffusion rates, and molecular sieving by size and/or shape exclusion. Packed bed separation is a typical adsorption-based separation method whereby selectivity arises from the thermodynamic equilibrium established upon interactions with adsorbing molecules, resulting in separation. Pore size and functionality play key roles in the separation performance of COFs. The functionality of COFs can be specifically tuned by introducing various functional sites on the organic building blocks *via* either pre-synthetic or post-synthetic modification. This allows a high degree of control over host–guest interactions to improve the adsorptive selectivity of COFs and facilitate the separation processes. Compared with other crystalline framework materials such as zeolites and MOFs, COFs possess one distinct advantage, *i.e.* facile membrane formation. The superior membrane performance and the selectivity of COFs can originate from the size-based selectivity or differing diffusion rates (kinetic separation). Tailoring the pore size of COFs can easily adjust the application of the kinetic-separation-based membranes from microfiltration to nanofiltration, and further to ultrafiltration. For a precisely defined aperture, COFs can be controlled in a large range of ways for separation of guest molecules with different van der Waals volumes. In this section, several strategies to prepare suitable COFs for separation application are discussed: (1) tailoring the pore size or shapes of COFs; (2) modifying pore surfaces with functional groups; (3) fabricating COF membranes.

2.1 Tailoring the pore size or shapes of COFs

The most efficient and convenient strategy to adjust the performance of separation media is to modify their pore size and shapes. Most COF materials are prepared *via* polymerization of rigid building blocks to create extended porous structures. The pore shape of COFs is determined by the topology of the porous networks, while pore size is governed by the length of the building blocks. For example, trigonal planar (C_3-symmetric) linkers can co-condense with C_3- or C_2-symmetric monomers to form two-dimensional (2D) sheets with a hexagonal topology, while tetragonal linkers co-condense with C_4- or C_2-symmetric monomers mainly to form a tetragonal topology.[57] In 2D COF structures, these 2D sheets stack *via* $\pi\cdots\pi$ interactions to generate pre-designed one-dimensional (1D) regular channels running along the stacking direction. Other than 2D COFs, three-dimensional (3D) COFs are also possible; however, they are still very rare and limited to $\sim$7 topologies.[46,97] Therefore, the current studies using COFs for separation application mainly focus on 2D COFs.

Within 2D COF structures, changing the length of building units may allow pore sizes to vary from micropores to mesopores (Fig. 3). For example, boroxine-linked COF-1 with a 1.5 nm pore

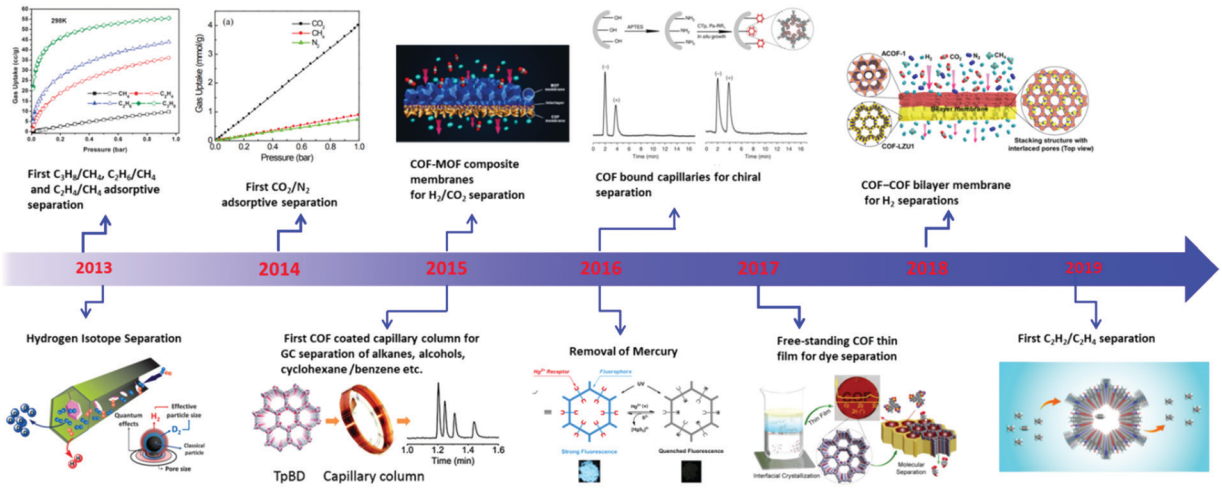

Fig. 2 Timeline for the advances in separation applications of COF-based adsorbents and membranes.

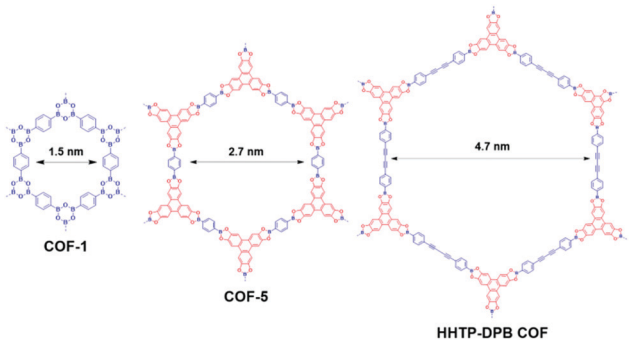

Fig. 3 Assembly of 2D hexagonal COFs (COF-1, COF-5, and HHTP-DPB COF) from building units with different sizes.

diameter was prepared by the heating of 1,4-benzenediboronic acid at 120 °C for 72 h. Condensation of 1,4-benzenediboronic acid and hexahydroxy triphenylene (HHTP) resulted in boronate ester-linked COF-5 which offered a larger pore of 2.7 nm.[63] When using the much longer monomer of 4,4′-diphenylbutadiynebis(boronic acid), a HHTP-DPB COF with a pore diameter of 4.7 nm was obtained.[98] Along the same line, Banerjee and coworkers[93] synthesized a series of COF thin films with pore diameters ranging from 1.4 nm to 2.6 nm by adjusting the molecular structure and length of the organic linkers.

Up to now, the pore size of reported 2D COFs typically has ranged from 0.64 nm to 5.8 nm, which were all larger than the kinetic diameter of targeted separating molecules such as gas (0.25–0.5 nm), water (0.26 nm) and C1–C4 alcohols (0.38–0.51 nm). To achieve high separation efficiency, the introduction of large side groups into COFs has proved to be an efficient approach to reduce the pore size of COFs. Han and co-workers[99] used tetra-fluoroterephthalonitrile as the building block to directly synthesize a perfluorinated covalent triazine-based framework (FCTF-1). Compared with the unfluorinated CTF-1, FCTF-1 displayed significantly reduced pore size, from microporous to ultra-microporous (<0.5 nm), and resulted in improved CO_2/N_2 selectivity in a mixed gas breakthrough test.

The direct integration of large side groups into COF structures is often challenging due to the increased steric hindrance that hinders the crystallinity of the COF structures. Therefore, post-synthetic modification is seen as an attractive method to adjust the pore size of 2D COFs, as shown in the pioneering work conducted by Jiang and co-workers in 2011.[100] In this study, the azide-containing COF-5 was first synthesized by a three-component condensation reaction with hexahydroxytriphenylene as the corner and a mixture of azide-appended benzene diboronic acid and 1,4-benzenediboronic acid as the pore walls (Fig. 4). Subsequently, the azide groups on the COF walls were used in click reactions with alkynes to form triazole-linked groups on the wall surfaces of COFs. When the content of the triazole-linked groups increased from 5% to 100%, a sharp decrease in pore sizes from 3.0 nm to 1.2 nm was observed for the modified COFs.

2.2 Modifying pore surfaces with functional groups

Besides pore shape and size, the pore environment also plays an important role in the separation performance of COFs. For example, Wang and co-workers[101] synthesized three isostructural 3D-TPB-COFs through the use of different functional groups with –H, –Me, or –F substituents. The COFs' pore environments were precisely tuned that led to different selectivities for CO_2 over N_2. The introduction of functional groups into COF pores can enhance the affinity and selectivity of COFs towards target compounds. For example, attaching chiral moieties onto the pore surfaces can endow achiral COFs with chiral separation properties. As shown in Fig. 5, there are two major approaches to introduce functional moieties into the COF skeletons: a bottom-up synthetic approach[102,103] and a post-synthetic modification approach.[104]

The bottom-up approach has been proved to be a facile and straightforward strategy to construct functional COFs. For this approach, the pre-designed functional groups are first installed on the monomers which then directly construct the target COFs. The advantage of this approach is the fact that the added functional groups can be homogeneously distributed along the

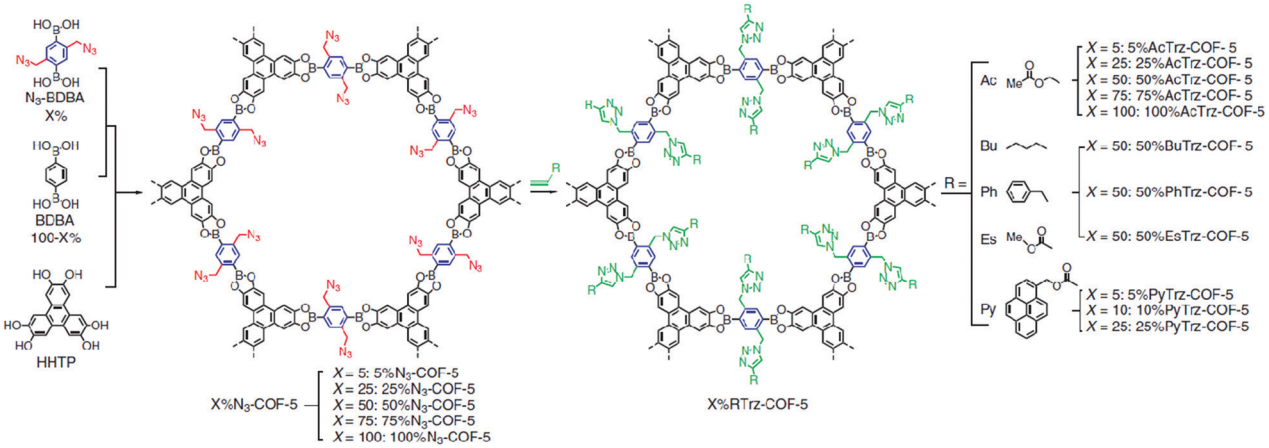

Fig. 4 The scheme shows a feasible strategy for the surface engineering of COFs through the combination of condensation reaction and click chemistry. Reproduced with permission from ref. 100. Copyright 2016, Springer Nature.

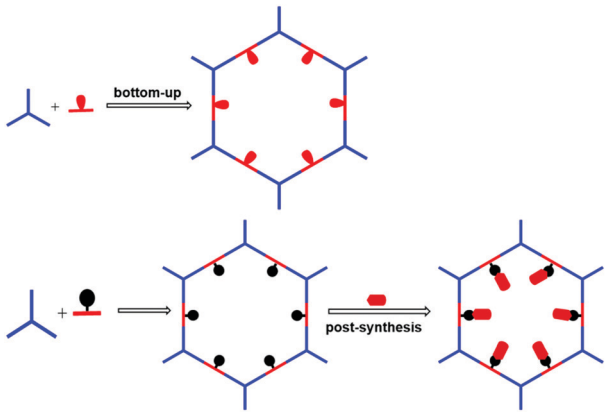

Fig. 5 General strategies to introduce functional moieties onto the COF skeletons. The red ovals represent the functional moieties.

COF surface and the number of functional groups can be precisely adjusted. However, functional COFs are difficult to obtain because the functional building block must simultaneously meet the demand of structural regularity (*e.g.* structural crystallinity) and porosity of the COFs. Nevertheless, the bottom-up strategy has achieved some success in constructing functional COFs for separation applications. For example, Yan and co-workers[94] synthesized chiral COFs by a bottom-up strategy and developed an *in situ* growth approach to prepare chiral COF capillary columns for chiral separation (Fig. 6). In this study, an enantiomer of (+)-diacetyl-l-tartaric anhydride was firstly utilized to react with 1,3,5-triformylphloroglucinol (Tp) to form chiral functionalized building blocks, CTp. CTp was then co-condensed with a diamine to afford chiral COFs which showed high resolution for enantiomer separation. Rather than modifying the pore surface with a neutral functional group, ionic COFs constructed *via* incorporating cationic monomers in the framework were also used as ideal materials for separation applications. In 2017, Qiu *et al.*[105] synthesized two 3D ionic COFs with a 3-fold interpenetrated network of dia topology. Condensation of tetrakis(4-formylphenyl)methane as a tetrahedral neutral linker and diimidium bromide/ethidium bromide as linear ionic building units afforded two novel 3D ionic COFs which not only possessed remarkable CO_2 uptake capacities but also showed quick removal of nuclear waste model ions and excellent size-selective capture for anionic dye ions.

As large functional groups usually hinder the formation of crystalline frameworks in the bottom-up synthesis approach, a post-synthetic strategy has emerged as an alternative. This approach allows for chemical and structural modification of the pore environment while maintaining the high porosity and crystallinity of the COF starting material. As a classic example shown in Fig. 7, Jiang's group[106] has utilized this strategy to successfully prepare functional COFs *via* covalent bond formation. They first synthesized 2D square-like porphyrin COFs ($[HO]_{x\%}$-H_2P-COFs) as a scaffold with phenol units on the pore walls to demonstrate structural functionalization of COFs. Carboxylic acid groups can be decorated on the inner channel walls of the COFs by a ring-opening reaction with succinic anhydride which was shown to enhance the adsorption capacity for CO_2.

2.3 Fabricating COF membranes

Membrane separation has demonstrated many advantages in the field of separation such as energy-efficiency, easy operation, low cost, and environmental friendliness.[107–110] The rational design of COF-based membranes for precise and rapid membrane separation has attracted continuous attention in the past decade. According to the components, COF membranes can be divided into two major types: COF-based mixed matrix membranes (MMMs) and pure COF membranes.

2.3.1 COF-Based MMMs. COF-based MMMs are fabricated *via* mixing COFs, in the form of nanoparticles or nanosheets, with a polymer matrix. COFs as porous fillers are blended into polymeric matrix membranes to gain additional passage for gases, water, and solvents to pass through, and enhance the permeability or selectivity. Compared to traditional inorganic or inorganic–organic hybrid materials (*e.g.* MOFs and zeolites), the pure organic nature of COFs endowed them with greater

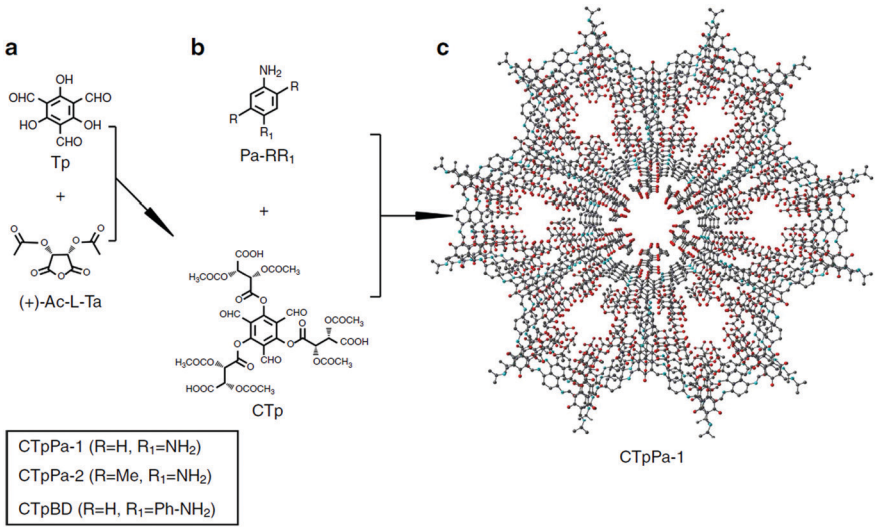

Fig. 6 The synthesis route of the CTpPa-1 COF for chiral separation. Reproduced with permission from ref. 94. Copyright 2016, Springer Nature.

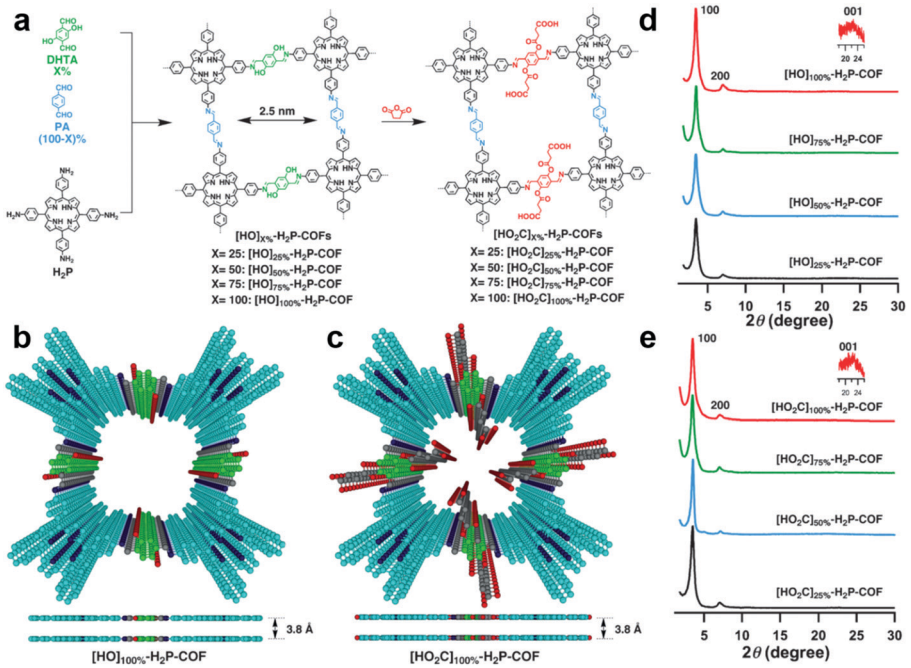

Fig. 7 (a) Synthesis of $[HO_2C]_{X\%}$-H_2P-COFs with channel walls functionalized with carboxylic acid groups through the ring opening reaction. Top views of (b) $[HO]_{100\%}$-H_2P-COF and (c) $[HO_2C]_{100\%}$-H_2P-COF. XRD patterns of (d) $[OH]_{X\%}$-H_2P-COFs and (e) $[HO_2C]_{X\%}$-H_2P-COFs. Reproduced with permission from ref. 106. Copyright 2017, Wiley-VCH.

compatibility with the polymer matrix used for membrane preparation.[111] For example, in a pioneering work,[112] self-supported TpBD@PBI-BuI and TpPa-1@PBI-BuI hybrid membranes were fabricated *via* the solution casting method. In this approach, spherical flower-like COF nanoparticles (TpBD and TpPa-1) were firstly prepared as an active phase. The polymer (PBI-BuI) solution in DMAc was mixed with the stock suspension of COFs by stirring and sonication to obtain a homogeneous suspension. The mixture was then poured on a clean glass surface and baked at 85 °C for 16 h. The membrane was peeled off and vacuum dried at 100 °C for 24 h before evaluating gas separation performance. The compatibility between the ketoenamine-linked COFs and PBI-BuI was remarkably improved by creating intermolecular interactions between H-bonded benzimidazole groups of PBI and COFs. Because the COF pores (1.8 nm for TpBD and 1.5 nm for TpPa-1) are much larger than the kinetic diameters of gases (3.3 Å for CO_2, 3.8 Å for CH_4), molecular sieving of gas molecules is not really expected from these COFs. Introduction of porous COF particles into polymers can lower the diffusion resistance and

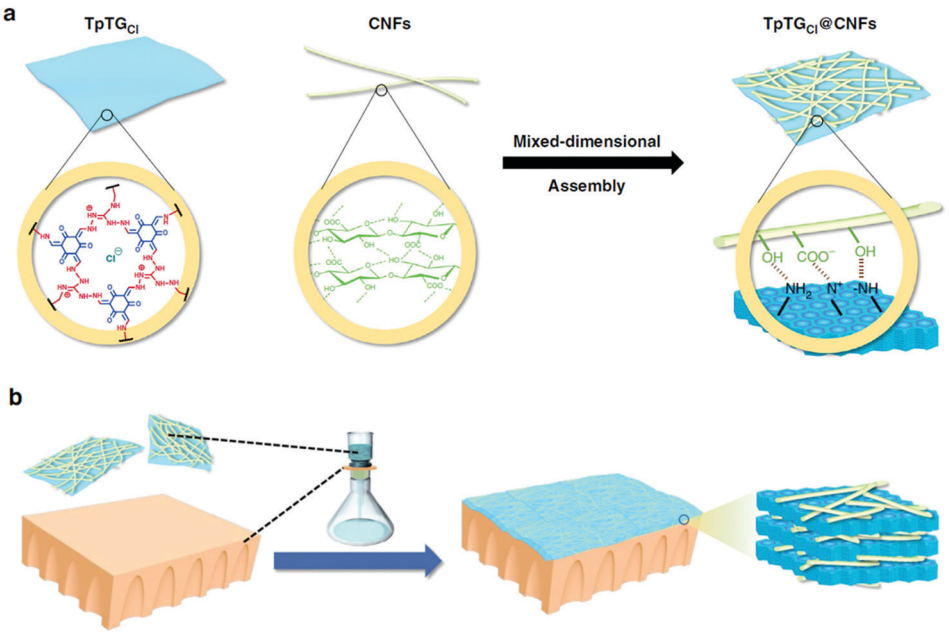

Fig. 8 (a) A schematic illustration showing the assembly process and the interactions between the 2D nanosheet and the 1D nanofiber. (b) A schematic illustration showing the vacuum-assisted self-assembly and the mixed-dimensional nanostructure. Reproduced with permission from ref. 117. Copyright 2019, Springer Nature.

thus elevate gas permeability. The TpBD(50)@PBI-BuI-based membranes showed the best CO_2 (14.8) and CH_4 (0.3) permeability, with high CO_2/CH_4 selectivity (48.7).

Along the same line, various COF-based MMMs, such as COF-1,[113] ACOF-1,[114] NUS-2,[115] NUS-3,[115] and SWM-1,[116] have been reported *via* a similar synthetic strategy and used for gas separation or water purification and desalination in the past three years. Very recently, Jiang and co-workers[117] proposed a type of mixed-dimension COF membrane using 2D COF nanosheets and 1D cellulose nanofibers (CNFs) as building blocks (Fig. 8). Briefly, in the first step, a Schiff-base COF, TpTGCl, was prepared by the condensation of triaminoguanidinium chloride (TGCl) with 1,3,5-triformylphloroglucinol (Tp), and was then exfoliated to obtain 2D nanosheets as the 2D component. TEMPO-oxidized CNFs with abundant carboxylic groups on their surface were employed as the 1D component. Subsequently, mixed-dimensional TpTGCl@CNFs-X nanocomposites with a planar TpTGCl nanosheet covered with dense networks of 1D CNFs were formed *via* blending the TpTGCl and CNFs in an aqueous solution, which can be easily dispersed in water to form a stable colloidal solution. Finally, a dense and defect-free TpTGCl@CNFs-X membrane was fabricated by a vacuum-assisted self-assembly on a polyacrylonitrile (PAN) substrate. By just varying the volume of the filtrate, their thickness can be tuned from dozens of nanometers to a few microns. Notably, the sheltering effect of CNFs was to effectively reduce the size of pores of the TpTGCl framework from 1.3 nm to 0.45–1.0 nm, which resulted in membranes capable of precise molecular sieving for salt rejection, alcohol dehydration, and dye rejection. Furthermore, the mechanical strength of the TpTGCl@CNFs-X membranes was improved compared with the pristine CNF membrane and the pristine TpTGCl membranes owing to the multiple interactions between the 2D membrane and 1D nanofibres.

Although the MMM approach showed advantages such as feasible operation and high generality to various COFs, the insufficient interfacial compatibility between COF nanofillers and polymers would often result in the occurrence of voids and defects, forming discontinuous membranes, which cannot fulfil the potential of the pore structure of COFs for membrane separation. Moreover, the poor interaction between the polymer matrix and fillers causes the precipitation and agglomeration of fillers during membrane formation and reduces the mechanical performance and processability of the polymer. Therefore, rational design and fabrication of continuous and pure COF membranes is an alternative approach to maximize the advantages of the pore structures of COFs as so to achieve the optimized separation performance.

2.3.2 Pure COF membranes. The bottom-up strategy has been widely used for the fabrication of continuous COF membranes or thin films.[118–122] Dichtel and co-workers[123] pioneered research on the growth of continuous COF films on substrates *via* a bottom-up method under solvothermal conditions. Briefly, HTTP (16 mg, 0.049 mmol) and 1,4-phenylenebis(boronic acid) (25 mg, 0.15 mmol) were added to a 15 mL cylindrical pressure vessel and were suspended in a mixed solution of mesitylene and dioxane (v/v 1 : 1; 1.0 mL). The mixture was sonicated for 30 min and a single-layer graphene (SLG)/Cu substrate was added. The sealed vessel was heated at 90 °C to form continuous COF-5 thin films on the graphene surface (Fig. 9). Synchrotron X-ray diffraction analysis demonstrated that the formed COF-5 films exhibited high crystallinity in comparison with the powdery samples. Particularly, this study showed that various supporting substrates can be applied, such as SLG/SiO_2 and SLG/SiC.

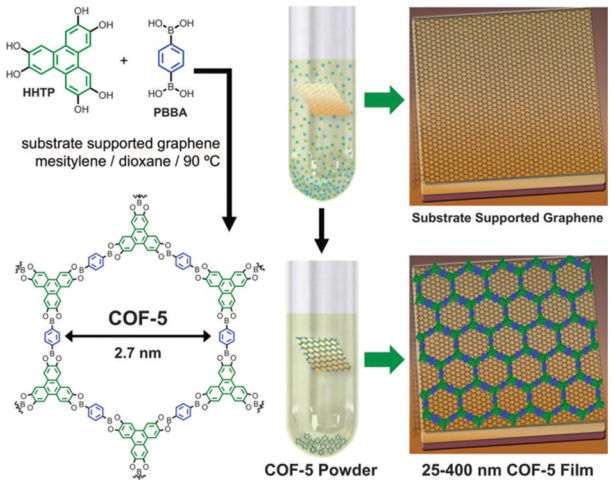

Fig. 9 Solvothermal condensation of HHTP and 1,4-phenylenebis-(boronic acid) in the presence of a substrate-supported SLG surface providing COF-5 as a film on the graphene surface. Reproduced with permission from ref. 123. Copyright 2011, American Association for the Advancement of Science.

To date, significant works have been done toward the development of continuous COF membranes on various supports and interfaces including MOFs and Al_2O_3 *via* the bottom-up strategy to achieve mixture separation.[91,124,125] However, these COF membranes show limited applications due to their requirement of physical supports. Recently, methods including interfacial polymerization,[126,127] the use of *p*-toluene sulfonic acid (PTSA) as a molecular organizer[128] and vacuum filtration[129] have been employed to fabricate pure COF membranes. Banerjee and co-workers[93] first reported a bottom-up interfacial crystallization method to prepare thin films under ambient conditions (Fig. 10). In this study, three layers of solvents were employed to fabricate COF thin films in a glass beaker. For example, 100 mL of dichloromethane containing Tp (0.075 mmol) as a bottom layer, 60 mL of pure water as the middle layer, and Bpy (0.112 mmol)–PTSA (0.224 mmol) salt dissolved in 100 mL of water (70 mL of water and 30 mL of acetonitrile) as the topmost layer were employed to fabricate Tp–Bpy thin films. A liquid–liquid interface was then formed between the immiscible water and dichloromethane. The Tp–Bpy thin films were grown by the polycondensation of Tp with Bpy–PTSA at the interface under static conditions for 72 h. Hydrogen bonding within the PTSA–amine salt solution decreased the diffusion rate of amine building blocks allowing the reaction rate to be minimized for thermodynamically-controlled crystallization to avoid the formation of amorphous polymers. Notably, these freestanding membranes can be transferred to various substrates to realize further applications. For example, the Tp–Bpy membrane, with a highly porous structure displayed remarkable solvent-permeance and solute-rejection performance.

Most of the freestanding COF thin films or membranes have been obtained by polymerization based on small rigid monomers; however, they typically show relatively weak mechanical properties that greatly hinder their further application. In order to improve mechanical performance, we first used linear polymers as building blocks to synthesize a series of polymer-covalent organic framework (polyCOF) hybrid membranes.[130] In this study, poly$_x$COF-42 membranes were prepared by a three-component condensation reaction of 1,3,5-triformylbenzene (TB) with a PEGylated linear polymer (DTH-400 or DTH-600) and 2,5-diethoxyterephthalohydrazide (DTH) in a designated molar ratio (x = 1/6, 2/6, 3/6, 4/6, 5/6 and 6/6) *via* an interfacial polymerization at room temperature (Fig. 11). The hydrazine moieties (DTH + DTH-400) (total amount: 0.0375 mmol) were first dissolved in a mixed solution of H_2O

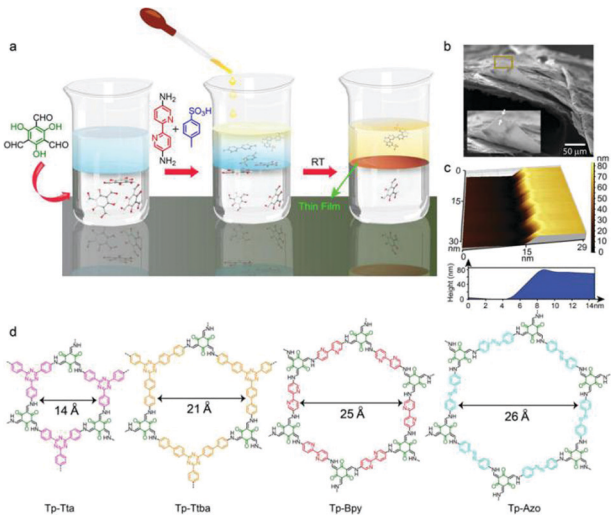

Fig. 10 (a) Schematic representation of the interfacial crystallization process used to synthesize the Tp–Bpy thin film. (b) SEM and (c) AFM images of the synthesized Tp–Bpy thin film. (d) Structures of COFs. Reproduced with permission from ref. 93. Copyright 2014, American Chemical Society.

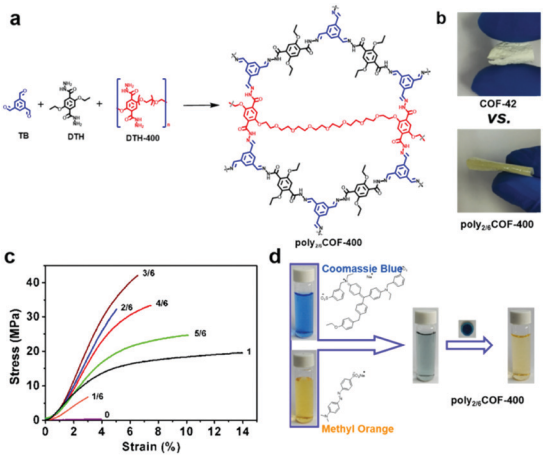

Fig. 11 (a) Strategy to fabricate polyCOF membranes *via* a three-component condensation. (b) Comparison of the mechanical properties of COF-42 *vs.* poly$_{2/6}$COF-42. (c) Stress–strain curves of poly$_x$COF-42 membranes with different polymer contents (x = 1/6, 2/6, 3/6, 4/6, 5/6, 1) compared with the COF-42 membrane. (d) Separation of Coomassie brilliant Blue R-250 and methyl orange dye solution by filtration with a poly$_{2/6}$COF-42 membrane. Reproduced with permission from ref. 130. Copyright 2019, American Chemical Society.

and dioxane (v/v 1 : 1; 2.0 mL) as a bottom layer in the beaker. Meanwhile, TB (0.025 mmol, 4.0 mg) was dissolved in a mixed solvent of 3 mL of mesitylene and 525 μL of CH_3COOH as an upper layer. The polymerization reaction of aldehyde and hydrazine takes place at the interface to afford polyCOF membranes at room temperature under static conditions for 48 h. The obtained polyCOF membrane not only inherited the advantages of COFs such as high crystallinity and porosity but also inherited the advantages of polymers such as good processability and high mechanical performance comparable to some commercial or classic polymeric membranes (*e.g.*, PVDF, PIM-1). Furthermore, the introduction of PEGylated polymer linkers into polyCOF membranes was found to effectively tailor COF pore sizes (from 2.4 nm to 1.3 nm), endowing the membranes with a molecular sieving effect for molecular separation. A mixed feed of methyl orange (M_w = 327 g mol^{-1}; ~1.1 nm × 0.4 nm) and Coomassie brilliant blue R-250 (M_w = 854 g mol^{-1}; ~1.8 nm × 2.3 nm) was passed through the poly$_{2/6}$COF-400 membrane. It selectively allowed the passage of methyl orange and completely rejected the large size of Coomassie brilliant blue R-250.

Recently, 3D-printing technology[131] has been successfully applied to the fabrication of robust heterogeneous COF monoliths. In this study, Pluronic F127 as a 3D-printing template was introduced to co-assemble with imine polymers in an aqueous environment to afford 3D-printable hydrogels. After the removal of F127 and solvent annealing, the 3D printed COF monoliths possess good structural integrity, high crystallinity, hierarchical pores with high surface areas, and robust mechanical stability. This approach provides a facile method to fabricate complex COF devices, which could be used for future separation applications that require sophisticated 3D architectures.

3. Separation applications of COFs

COF-based adsorbents and membranes have been developed as multifunctional materials for diverse separation applications. According to the flow media of application fields, they are mainly classified into two categories: gas phase separation and liquid phase separation. In this section, the typical and emerging applications of COF-based separation media will be highlighted and discussed.

3.1 Gas phase separation

In the past decade, COFs have been touted as ideal materials for gas capture and separation applications. Some specific topics of gas separations in the petrochemical industry have been widely investigated, including hydrocarbon separation, CO_2 separation capture, separation of hydrogen isotopes, and H_2 purification. Usually, the adsorption of gas molecules mainly depends on the adsorption affinity between the gas molecules and pore walls. For pore size, especially nearing the size of the gas molecules, there will be additional interaction from the pore wall as well as the gas molecules adsorbed to the other sides. In order to specifically adsorb a certain gas molecule especially for gas separation, porous materials could be designed to possess pore size nearing the size of the gas molecule. In this section, the typical gas separation applications of COFs are highlighted and discussed in detail.

3.1.1 Carbon dioxide separation. Carbon dioxide (CO_2) capture and sequestration have attracted tremendous research attention due to growing concern about environmental issues such as air pollution and global warming.[132–134] Post-combustion flue gas at power plants, a major source of CO_2 emission, typically contains 15% CO_2 and 85% N_2. Because CO_2 and N_2 possess very close kinetic diameters of 3.3 Å and 3.64 Å, it is difficult to separate these two gases *via* molecular sieving. Therefore, adsorption-based separation methods, such as pressure swing adsorption, are the most efficient processes.[135–140] Developing new adsorbents with high CO_2 capacity and good CO_2/N_2 selectivity is a prime focus in this field.[141,142] Considering the different features of CO_2 and N_2 (quadrupole moments and polarizabilities), it is reasonable to design and synthesize CO_2-philic materials by introducing strongly basic sites such as imines, amines, triazines, and tetrazoles into the skeleton. Due to the low density, high porosity, and facile functionality, COFs have demonstrated high potential for CO_2/N_2 separation. Examples of COFs and their applications in CO_2/N_2 separation are summarized in Table 1. Among all reported COFs, nitrogen-rich COFs are considered to be ideal materials for CO_2 storage and separation, because the porous backbone with amine groups can improve the affinity to CO_2 and increase the CO_2 uptake capacity and selectivity.

In 2012, Banerjee's group[143] first synthesized two chemically stable COFs (TpPa-1 and TpPa-2) using reversible and irreversible routes to investigate CO_2 adsorption. TpPa-1 with a BET surface area of 535 m^2 g^{-1} was constructed from Tp with *p*-phenylenediamine (Pa-1) *via* the solvothermal synthesis showing a CO_2 uptake of 78 cm^3 g^{-1} at 273 K and 1 bar. Surface area, pore volume, and pore size play a significant role in the gas capture capability of COFs. For example, Wei and co-workers[144] synthesized TpPa-COF (MW) using a microwave-assisted solvothermal method which showed better crystallinity and higher BET surface area (725 m^2 g^{-1}) than the one prepared by conventional solvothermal synthesis (TpPa-1). The uptake of CO_2 of TpPa-COF (MW) was measured to be 111 cm^3 g^{-1} at 273 K, which was much higher than that of TpPa-1 (78 cm^3 g^{-1}). Notably, the isosteric enthalpy of adsorption (Q_{st}) was 34.1 kJ mol^{-1} at zero coverage and the adsorption selectivity for CO_2/N_2 calculated *via* the IAST (Ideal Adsorbed Solution Theory) method was 32 at 273 K. The high adsorption selectivity for CO_2/N_2 has been mainly attributed to the high surface area and the abundant N–H sites on the pore wall of TpPa-COF (MW) which can favourably interact with the polarizable CO_2 molecules through weak interactions such as hydrogen bonding interactions.

Recently, Lai and co-workers[145] synthesized thermally and chemically stable chlorine-functionalized CAA-COF-1 and CAA-COF-2 *via* a Schiff base condensation reaction involving 2,5-dichloro-1,4-phenylene diamine or 3,3'-dichlorobenzidine dihydrochloride with Tp. Notably, the as-synthesized CAA-COF-1 materials showed enhanced CO_2 adsorption capacity (by almost 28–44%) compared to their non-chlorinated counterparts

Table 1 Summary of selective CO_2/N_2 adsorption in COFs

COFs	BET surface [m^2 g^{-1}]	Pore size [nm]	CO_2 uptake [cm^3 g^{-1}][a]	Q_{st} [kJ mol^{-1}]	CO_2/N_2 Selectivity	Ref.
TaTp-1	535	1.3	78	—	—	143
TaTp-COF (MW)	725	1.3	111	34.1	32	144
ACOF-1	1176	0.94	90	27.6	40[c]	90
COF-JLU2	415	0.96	110	31.0	77	150
N-COF	1700	1.1	61.2	—	—	146
COF-TpAzo	1286	2.58	53.76	32.0	145	154
$[HO]_{25\%}$-H_2P-COF	1054	2.5	27	32.2	—	106
$[HO]_{50\%}$-H_2P-COF	1089	2.5	23	29.4	—	106
$[HO]_{75\%}$-H_2P-COF	1153	2.5	26	31.5	—	106
$[HO]_{100\%}$-H_2P-COF	1284	2.5	32	36.4	8	106
$[HO_2C]_{25\%}$-H_2P-COF	786	2.2	49	38.2	—	106
$[HO_2C]_{50\%}$-H_2P-COF	673	1.9	68	39.6	—	106
$[HO_2C]_{75\%}$-H_2P-COF	482	1.7	80	41.2	—	106
$[HO_2C]_{100\%}$-H_2P-COF	364	1.4	89	43.5	77	106
$[Et]_{25}$-H_2P-COF	1326	2.2	28	15.5	—	155
$[Et]_{50}$-H_2P-COF	821	1.9	23	15.3	—	155
$[Et]_{75}$-H_2P-COF	485	1.6	21	15.6	—	155
$[Et]_{100}$-H_2P-COF	187	1.5	19	15.3	—	155
$[MeOAc]_{25}$-H_2P-COF	1238	2.1	43	16.4	—	155
$[MeOAc]_{50}$-H_2P-COF	754	1.8	45	17.4	—	155
$[MeOAc]_{75}$-H_2P-COF	472	1.5	42	16.7	—	155
$[MeOAc]_{100}$-H_2P-COF	156	1.1	33	17.8	—	155
$[AcOH]_{25}$-H_2P-COF	1252	2.2	48	17.7	—	155
$[AcOH]_{50}$-H_2P-COF	866	1.8	60	17.8	—	155
$[AcOH]_{75}$-H_2P-COF	402	1.5	55	18.3	—	155
$[AcOH]_{100}$-H_2P-COF	186	1.3	49	18.8	—	155
$[EtOH]_{25}$-H_2P-COF	1248	2.2	47	18.2	—	155
$[EtOH]_{50}$-H_2P-COF	784	1.9	63	19.7	—	155
$[EtOH]_{75}$-H_2P-COF	486	1.6	60	19.2	—	155
$[EtOH]_{100}$-H_2P-COF	214	1.4	43	19.3	—	155
$[EtNH_2]_{25}$-H_2P-COF	1402	2.2	59	20.4	—	155
$[EtNH_2]_{50}$-H_2P-COF	1044	1.9	80	20.9	17[d]	155
$[EtNH_2]_{75}$-H_2P-COF	568	1.6	68	20.8	—	155
$[EtNH_2]_{100}$-H_2P-COF	382	1.3	49	20.9	—	155
CAA-COF-1	841	1.31	128	29.9	67[b]	145
CAA-COF-2	723	1.86	60	29.5	51[b]	145
3D-IL-COF-1	517	0.83	27.2[e]	—	24.6	161
3D-IL-COF-2	653	1.07	38.7[e]	—	24.0	161
3D-IL-COF-3	870	1.24	25.1[e]	—	24.4	161
3D-COF-1a	596	—	—	—	7.1	161
3D-IL-COF-1b	537	—	—	—	43.6	161

[a] Unless otherwise stated, the CO_2 capacity was measured at 273 K and 1 bar. [b] Determined using IAST with CO_2/N_2 (10 : 90 v/v) at 298 K and 1 bar. [c] Determined using IAST with CO_2/N_2 (10 : 90 v/v) at 273 K and 1 bar. [d] Determined using IAST with CO_2/N_2 (15 : 85 v/v) at 298 K and 1 bar. [e] The CO_2 capacity was measured at 298 K and 1 bar.

(TpPa-1 and TpBD), which can be attributed to the dipolar interactions between electron-rich chlorine atoms and electron-deficient carbon atoms of CO_2 (Fig. 12). The calculated Q_{st} values for CO_2 were 29.9 kJ mol^{-1} (CAA-COF-1), 26.3 kJ mol^{-1} (TpPa-1), 29.5 kJ mol^{-1} (CAA-COF-2), and 28.3 kJ mol^{-1} (TpBd), respectively, at zero loading. The IAST adsorption selectivity for CO_2/N_2 (273 K) was 83 (CAA-COF-1), 64 (CAA-COF-2), 53 (TaPa-1) and 44 (TpBd), for a 10/90 CO_2/N_2 gas mixture. Column breakthrough experiments were further performed to validate the CO_2/N_2 separation ability of CAA-COFs under dry and humid mixed gas conditions. Under dry mixed gas conditions, CAA-COF-1 exhibited a breakthrough selectivity of 95 for CO_2/N_2 (10/90 gas mixture), whereas for CAA-COF-2, the CO_2/N_2 selectivity was 54 under the same conditions.

In 2015, Zhao's group[146] reported an imine-based nitrogen-rich COF (N-COF) *via* a Schiff base reaction of two triangular building units of 1,3,5-triformylbenzene and 2,4,6-tris(4-aminophenyl)-1,3,5-triazine (TAPB). The CO_2 uptake capacity of N-COF at 1 bar was 61.2 cm^3 g^{-1} and 32.4 cm^3 g^{-1} for 273 K and 298 K, respectively. By contrast, the N_2 uptake capability was only 3.6 cm^3 g^{-1} (1 bar, 273 K), indicating a high adsorption selectivity toward CO_2 over N_2.

Among COFs with various bond linkages, the azine-linked COFs are good candidates for CO_2 capture due to the strong interaction of CO_2 with the azine linkages *via* the nitrogen atoms with lone pair electrons which can effectively enhance the adsorption capacity. Liu and co-workers[90] synthesized an azine-linked COF (ACOF-1) by the co-condensation of 1,3,5-triformylbenzene with hydrazine hydrate under solvothermal conditions. The BET surface area of ACOF-1 was calculated to be 1176 m^2 g^{-1} and the total CO_2 uptake capacity was 17.7 wt% at 273 K and 1 bar, which was higher than those of some reported COFs like TDCOF-5 (9.2 wt%, SABET = 2497 m^2 g^{-1}),[147] ILCOF-1 (6.0 wt%, SABET = 2723 m^2 g^{-1}),[148] COF-103 (7.6 wt%, SABET = 3530 m^2 g^{-1}),[149] and COF-5 (5.9 wt%, SABET = 1670 m^2 g^{-1})[149] under the same test conditions. The Q_{st} value

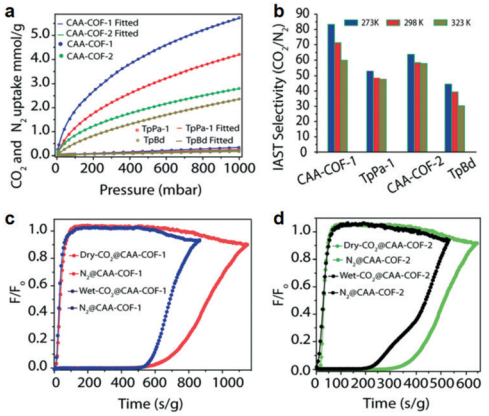

Fig. 12 (a) CO_2 and N_2 adsorption isotherms at 273 K and fitted data for CAA-COF-1, TpPa-1, CAA-COF-2, and TpBd; (b) CO_2/N_2 IAST selectivity at 273, 298 and 323 K for a 10/90 CO_2/N_2 feed mixture; (c and d) column breakthrough experimental results for CAA-COF-1 and -2 using a 10/90 CO_2/N_2 feed mixture under dry and humid conditions at 298 K. Reproduced with permission from ref. 145. Copyright 2018, Royal Society of Chemistry.

for CO_2 was 27.6 kJ mol^{-1} at zero coverage, calculated from the adsorption isotherms at 273 and 298 K. The IAST selectivity for CO_2/N_2 was 40 at 273 K. The good adsorption selectivity for CO_2 over N_2 can be attributed to the abundant nitrogen atoms on the pore wall of ACOF-1, which can enhance the binding affinity to CO_2.

Along the same line, the same group[150] reported an azine-linked COF (COF-JLU2) with abundant heteroatom sites in the COF skeleton through a condensation reaction of Tp and hydrazine hydrate (Fig. 13). Remarkably, COF-JLU2 showed a CO_2 uptake of 21.7 wt% at 273 K and 1 bar, which is not only higher than those of some reported COFs such as COF-103, TDCOF-5 and ACOF-1, but also comparable to those of some amorphous porous organic polymers such as CPOP-1 (21.2 wt%, BET = 2220 m^2 g^{-1}),[151] imine-linked porous polymer PPF-1 (26.7 wt%, BET = 1740 m^2 g^{-1}),[152] and azo-linked polymer ALP-1 (23.6 wt%, BET = 1235 m^2 g^{-1}).[153] The Q_{st} of COF-JLU2 for

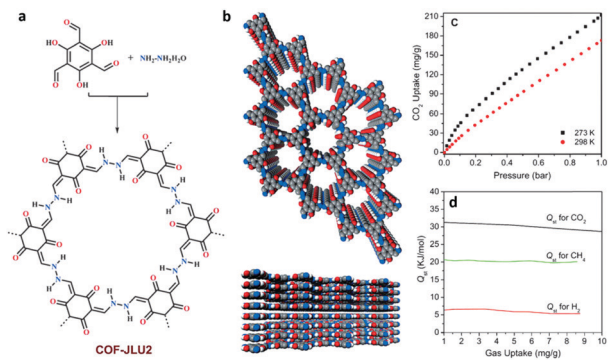

Fig. 13 (a) Schematic representation of the synthesis of COF-JLU2. (b) Top and side views of the AA stacking structure of COF-JLU2. (c) CO_2 sorption measurements for COF-JLU2. (d) Isosteric heats of adsorption for COF-JLU2. Reproduced with permission from ref. 150. Copyright 2015, Wiley-VCH.

CO_2 was 31 kJ mol^{-1} at low coverage which was higher than the value reported for ACOF-1 (27.6 kJ mol^{-1}). Furthermore, the estimated adsorption selectivity for CO_2/N_2 was 77, as determined by Henry's law in the 0 to 0.1 bar pressure range, which surpassed most carbon-based materials such as ACOF-1 (40) or imine-linked porous polymers PPFs (21). COF-TpAzo,[154] an azo-based (N=N) COF, was synthesized as a stable 'CO_2-philic' and 'N_2-phobic' adsorptive separation material *via* a Schiff base condensation reaction between 4,4′-azodianiline and Tp. The CO_2 adsorption capacity of COF-TpAzo reached up to 105.6 mg g^{-1}. The high adsorption can be attributed to the cooperative interactions between CO_2 molecules and azo/imine groups in the COF skeleton. The Q_{st} for CO_2 can reach up to 32.0 kJ mol^{-1} at zero coverage. Based on the initial slope calculation in the low pressure range, COF-TpAzo exhibited high adsorption selectivities for CO_2/N_2 of 127 at 273 K and 145 at 298 K.

Anchoring functional groups on the pore walls that can interact with CO_2 is also an effective strategy to increase the adsorption capacity and separation efficiency. For example, Jiang's group[104] introduced carboxylate groups onto the pore surface of COFs by a post-synthetic modification approach to increase the affinity towards CO_2. Adopting a similar strategy, the same group[155] introduced alcohol, alkyl chains, carboxylic acid, ester, and amine units onto the pore wall of an imine-linked porphyrin COF through click reactions between the azide compounds and ethynyl units (Fig. 14). The pore surface engineering resulted in a decrease of the BET surface area, pore size, and pore volumes of functionalized COFs compared with their parent COFs. For example, as the ethyl content x in $[Et]_x$-H_2P-COFs increased from 25 to 100, the BET surface area decreased from 1326 to 187 m^2 g^{-1}, the pore volume changed from 0.55 to 0.18 cm^3 g^{-1}, and the pore size decreased from 2.2 to 1.5 nm. Similarly, $[MeOAc]_xH_2P$-COFs, $[EtNH_2]_x$-H_2P-COFs, and $[AcOH]_x$-H_2P-COFs also showed the same tendencies. Introducing ethyl units onto the pore walls, the resulting $[Et]_x$-H_2P-COFs with low CO_2 adsorption capacities were similar to the $[HC{\equiv}C]_x$-H_2P-COFs. But introducing ester units ($[MeOAc]_x$-H_2P-COFs), hydroxyl groups ($[EtOH]_x$-H_2P-COFs), carboxylic acid groups ($[AcOH]_x$-H_2P-COFs), and amino groups ($[EtNH_2]_x$-H_2P-COFs), these COFs exhibited enhanced CO_2 adsorption capacities. The Q_{st} value of CO_2 increased in the order $[EtNH_2]_x$-H_2P-COFs (20.4–20.9 kJ mol^{-1}) > $[EtOH]_x$-H_2P-COFs (18.2–19.3 kJ mol^{-1}) > $[AcOH]_x$-H_2P-COFs (17.7–18.8 kJ mol^{-1}) > $[MeOAc]_x$-H_2P-COFs (16.4–17.8 kJ mol^{-1}) > $[HC{\equiv}C]_x$-H_2P-COFs ≈ $[Et]_x$-H_2P-COFs (15.3–16.8 kJ mol^{-1}). Breakthrough simulations of $[EtNH_2]_{50}$-H_2P-COFs had a breakthrough time of 25, which was much longer than that of $[HC{\equiv}C]_{50}$-H_2P-COFs (7).

In addition, COF-based membranes for CO_2/N_2 separations have been reported.[156–158] A computational study based on few-layered 2D-COF membranes was conducted to explore their capability for CO_2/N_2 separations in 2016.[159] This study revealed that the narrow interlayer passages formed between the stacked nanosheets have a 'gate-closing' effect on the selective transport of molecules. Tuning the stacking modes of COF nanosheets to construct a favorable energetic microenvironment resulted in a high permeability of CO_2 and a high

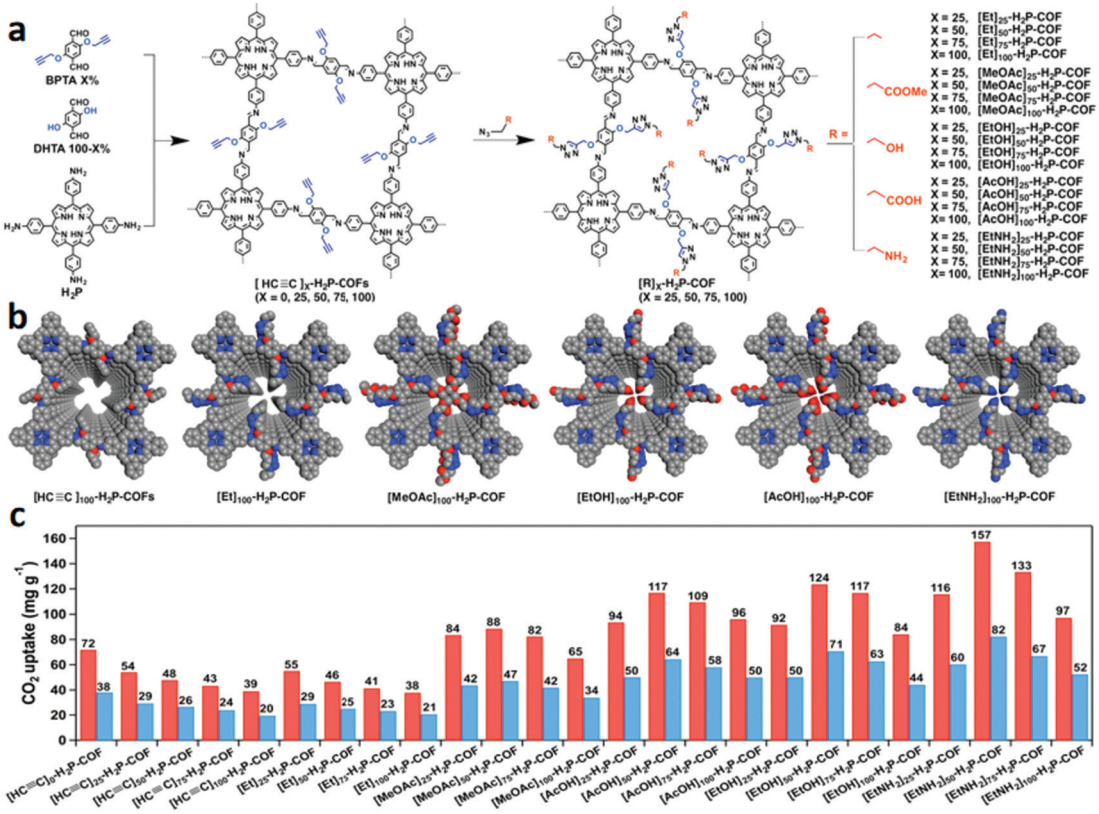

Fig. 14 (a) Schematic of pore surface engineering of imine-linked COFs with various functional groups *via* click reactions; (b) pore structures of COFs with different functional groups; (c) CO_2 adsorption capacity of the COFs at 273 (red) and 298 K (blue) and 1 bar. Reproduced with permission from ref. 155. Copyright 2015, American Chemical Society.

CO_2/N_2 selectivity. In 2017, an experimental study of CO_2/N_2 separation by the PEBA-based MMMs with 1 wt% COF nanosheet clusters showed a high CO_2/N_2 gas selectivity of 64.[160]

3.1.2 Methane purification. Methane (CH_4) is a promising substitute for conventional fossil fuels due to its advantages such as abundant natural reserves and low pollution.[161–164] However, CH_4 is usually contaminated with CO_2 which will reduce its heat value and energy content. Therefore, it is desirable to remove CO_2 from CH_4 before transporting and utilizing natural gas. The adsorption-based separation method has demonstrated high potential for this separation process.[165–169] For instance, nitrogen-rich COFs not only can selectivity capture CO_2 over N_2, but also have a high adsorption selectivity for CO_2/CH_4 due to the relatively low adsorption capacity of CH_4 under ambient conditions. The IAST sorption selectivity for the CO_2/CH_4 mixture calculated for COF-TpAzo, COF-JLU2, ACOF-1, CAA-COF-1, and CAA-COF-2 are 39, 4.1, 37, 29 and 19 at 273 K, respectively.

Besides adsorption-based separation, COF-based membrane separation has also been performed for CO_2/CH_4 separation. In 2018, Caro and co-workers[124] reported a continuous 2D azine-linked ACOF-1 membrane on a porous a-Al_2O_3 support for CO_2/CH_4 separation (Fig. 15). Due to the synergistic effect of effective molecular sieving of CH_4 and excellent CO_2 adsorption capacity by stacked pores of ACOF-1, this membrane exhibited a high selectivity of 86.3 for the CO_2/CH_4 mixed gas and a favorable CO_2 permeance of about 9.9×10^{-9} mol m^{-2} s^{-1} Pa^{-1}. The overall performance exceeded the Robeson upper bound (2008) for CO_2/CH_4. Moreover, this COF membrane demonstrated long-term operational and high hydrothermal stability owing to the strong covalent azine bonds.

In addition, the separation of C2 hydrocarbon (C_2H_2 and C_2H_4) from CH_4 has also aroused tremendous attention. For example, Zhu and co-workers[88] synthesized a new microporous 3D COF, namely, MCOF-1. The uptake values of MCOF-1 are 9, 36 and 44 cm^3 g^{-1} for CH_4, C_2H_4, and C_2H_6, respectively, at 298 K and 1 bar. The Q_{st} values of CH_4, C_2H_4, and C_2H_6 are 15, 19 and 41 kJ mol^{-1}, respectively, at zero loading. Notably, the IAST adsorption selectivity of MCOF-1 for C_2H_6/CH_4 (88) and C_2H_4/CH_4 (26) exceeds those of the previously reported porous materials, such as UTSA-34b (18–24),[170] UTSA-35a (15–25),[171] La-PCP (22 for C_2H_6/CH_4 and 12 for C_2H_4/CH_4)[172] and mesoPOF (25–40),[173] at 298 K and 100 kPa. The narrow pore size of MCOF-1 (0.64 nm) does not allow C_2H_6 (0.44 nm) and CH_4 (0.37 nm) to enter the pore channel at the same time. C_2H_6 molecules first occupy most of the pore windows and suppress the entry of CH_4 for MCOF-1 preferring C_2H_6 which leads to exceedingly high selectivity for C_2H_6/CH_4.

As another example, Zhao *et al.*[174] prepared three isoreticular COFs (N-COF, P-COF, and T-COF) *via* Schiff base condensation reactions of 1,3,5-benzenetricarbaldehyde (BTCA) with three amine monomers of different planarity: tris(4-aminotriphenyl)amine (TAPA), TAPB and 2,4,6-tris(4-aminophenyl)-s-triazine (TAPT).

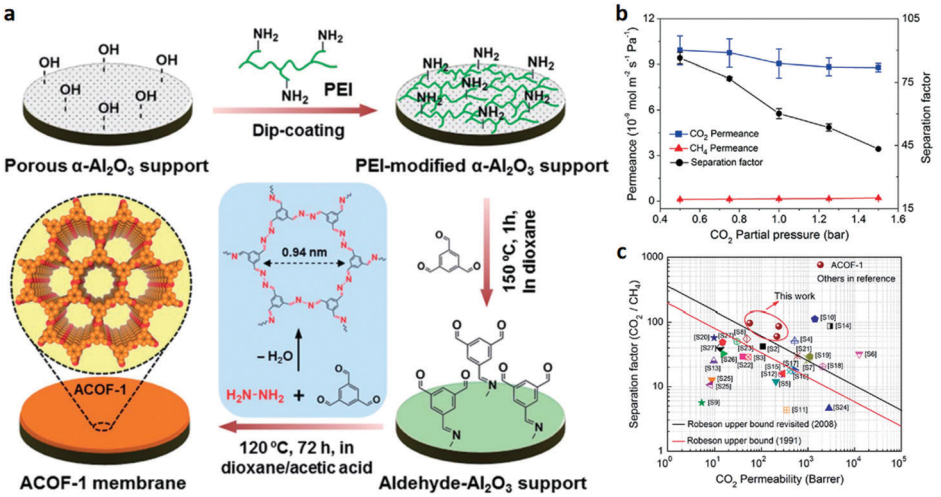

Fig. 15 (a) Schematic illustration of synthesizing the ACOF-1 membrane on the porous a-Al_2O_3 support. (b) CO_2 permeance and CO_2/CH_4 separation factor of the ACOF-1 membrane as a function of the CO_2 partial pressure at 120 °C. (c) Permeability *vs.* separation factor of various membranes and the upper bound correlation for CO_2/CH_4 separation. Reproduced with permission from ref. 124. Copyright 2018, Royal Society of Chemistry.

The PXRD and BET surface area measurements revealed that employing planar monomers can enhance the crystallinity and porosity of the resultant COFs (T-COF). In addition, the uptake values of CH_4 and C_2H_6 for T-COF are higher than those of N-COF and P-COF which are composed of non-planar linkages. In terms of gas separation, the IAST adsorption selectivity of N-COF (18.8) with the smallest pore size (~5.4 Å) exhibited a higher value than that of P-COF (12.1) and T-COF (10.0).

3.1.3 Separation of acetylene from ethylene. Unsaturated C2 hydrocarbons such as acetylene (molecular size: 3.32 × 3.34 × 5.70 Å) and ethylene (3.28 × 4.18 × 4.84 Å) are essential feedstocks in the petrochemical industry.[175,176] C_2H_4 is mainly produced by petrochemical cracking processes, in which C_2H_2 is present as a trace by-product. The trace C_2H_2 contaminant must be removed before C_2H_4 polymerization because it will poison the polymerisation catalyst by the formation of solid metal acetylides to block the fluid stream and even lead to an explosion. Current techniques to remove acetylene from ethylene include the partial hydrogenation of acetylene into ethylene and organic solvent extraction.[177] These processes suffer from high cost and low efficiency. On the other hand, adsorptive separation of C_2H_2 from the C_2H_2/C_2H_4 mixture is a promising alternative due to its much higher efficiency and lower cost.

Recently, the utilization of COFs as adsorbents for C_2H_2/C_2H_4 separation has been proved to be a promising alternative energy-efficient strategy.[178] For example, Han and co-workers[179] developed a porous COF, CTF-PO71, with functional sites on the pore surface to address the C_2H_2/C_2H_4 gas separation challenge. The C_2H_2 adsorption capacity of CTF-PO71 at 100 kPa was 104 and 74 $cm^3\ g^{-1}$ at 273 and 298 K, respectively, which are higher than those of C_2H_4 (78 and 49 $cm^3\ g^{-1}$) under the same conditions. The theoretical calculation results showed that C_2H_2 absorbed on all preventive sites (C═O group) on the pore surface of CTF-PO71 offered a higher binding energy than C_2H_4. Fixed-bed column breakthrough experiments were conducted to examine the real C_2H_2/C_2H_4 separation performance. The net breakthrough time of C_2H_4 and C_2H_2 was measured to be 7.77 and 1910 s, respectively, giving a C_2H_2/C_2H_4 separation factor of 246. Due to the stronger affinity of C_2H_2 to CTF-PO71, C_2H_2 molecules preferentially occupied almost all the adsorption sites and prevented C_2H_4 from effective adsorption in the cases of mixed gas that led to the high separation performance.

Zhu and co-workers[96] synthesized a crystalline naphthalene diimide COF (PAF-110) *via* imidization of triangular tris(4-aminophenyl)amine and linear naphthalene-1,4,5,8-tetracarboxylic dianhydride. The adsorption isotherms of acetylene and ethylene were measured at 273 K and 1 bar. The acetylene capacity of PAF-110 was 3.48 mmol g^{-1}, which was around two times higher than that of ethylene (1.61 mmol g^{-1}) under the same conditions. The Q_{st} values for acetylene and ethylene were estimated using the Clausius–Clapeyron equation. The Q_{st} values for C_2H_2 and C_2H_4 were 38.4 and 22.6 kJ mol^{-1}, respectively, at zero coverage. These results indicated that PAF-110 had a higher affinity to C_2H_2. A computational study suggested that the carbonyl oxygen atoms in PAF-110 have a stronger electrostatic interaction with hydrogen atoms in acetylene than in ethylene (Fig. 16). This result was consistent with the adsorption data and calculated Q_{st}. The IAST adsorption selectivity of C_2H_2 over C_2H_4 ranged from 3.9 to 8.0 at 298 K, which exceeded the selectivity (1.8 to 2.8) of CTF-PO71. Along the same line, the same group[180] prepared PAF-120 using 1,3,5-tris(4-aminophenyl) instead of TAPA to react with naphthalene-1,4,5,8-tetracarboxylic dianhydride. The adsorption capacities of PAF-120 for acetylene and ethylene were 3.50 and 1.89 mmol g^{-1}, respectively, similar to those of PAF-110. Notably, the adsorption selectivity for C_2H_2/C_2H_4 separation was 4.1, which was better than that of PAF-110 (selectivity: 3.9). These reports suggest that carbonyl-rich COFs could be used as ideal materials for C_2H_2/C_2H_4 separation ascribed to their stronger electrostatic interaction with acetylene than ethylene. In addition, some adsorbents with NH_2 and F groups also play important roles for

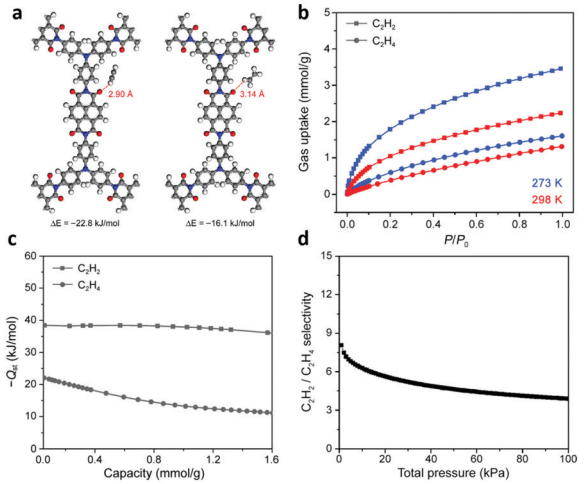

Fig. 16 (a) Optimized binding sites and binding energies for acetylene and ethylene within PAF-110. (b) Acetylene and ethylene adsorption isotherms for PAF-110 at 273 K (blue symbols) and 298 K (red symbols). (c) Q_{st} curves for acetylene and ethylene. (d) Acetylene/ethylene adsorption selectivity of PAF-110 at 298 K, as determined from ideal adsorbed solution theory. Reproduced with permission from ref. 96. Copyright 2018, American Chemical Society.

the preferential binding with C_2H_2 over C_2H_4 by the weak acid–base interaction between $-NH_2$ and C_2H_2 or strong C–H···F hydrogen bonding.[30]

3.1.4 Hydrogen purification. Hydrogen has been considered as an alternative clean energy source for conventional fuels in cars because of its clean combustion and high chemical energy density.[181,182] However, the H_2 product usually contains other gases (CO_2, N_2, CH_4, *etc.*) in industry.[183–186] Therefore, exploring some strategies for highly efficient H_2 purification is urgently needed. Taking H_2/N_2 and H_2/CH_4 as typical examples, it is relatively difficult to use packed bed technologies to separate them because most adsorbents showed low adsorption ability for H_2, N_2, and CH_4 under ambient conditions. The advantages of well-defined pore aperture, ordered channel structure, large surface area and permanent porosity make COFs excellent candidates for using as molecular sieving membranes.[187–192] For example, Gao and co-workers[193] first developed a COF-320 membrane on a porous a-Al_2O_3 substrate surface. A uniform and compact COF-320 membrane with a thickness of ~4 μm was obtained. Gas permeation experiments were carried out using H_2 (0.28 nm), CH_4 (0.37 nm), and N_2 (0.38 nm), for 3D COF-320 membranes, and the permeation flux was increased as $H_2 > CH_4 > N_2$. The permselectivity for H_2/CH_4 (2.5) and H_2/N_2 (3.5) is closely similar to the theoretical calculation results (2.83 for H_2/CH_4, 3.74 for H_2/N_2) governed by the Knudsen diffusion mechanism. Therefore, the gas transport is mainly governed by the Knudsen diffusion for the 3D COF-320 membrane.

Compared to the 3D COFs, 2D COFs in the form of layered sheets within well-ordered in-plane pores favoured the construction of membranes with minimal transport resistance. As discussed above, the pore size of most COFs (0.8–5 nm) is remarkably larger than the kinetic diameter of common gas molecules (0.25–0.5 nm). Thus, it is difficult to fabricate sieving COF membranes for gas separations. To address this issue, Caro and co-workers[194] developed an Al_2O_3 supported COF-LZU1-ACOF-1 bilayer membrane *via* an *in situ* growth method. In their study, the surface Al_2O_3 disk was sequentially treated with 3-aminopropyltriethoxysilane (APTES), TFB and *p*-phenylenediamine (PDA)/hydrazine hydrate mixture (Fig. 17). The obtained dual-amino-functionalized Al_2O_3 disk allowed the COF-LZU1 layer to grow on the support surface by condensation of TFB with PDA at room temperature, and then an ACOF-1 layer was synthesized by condensation of the residual amount of TFB and hydrazine hydrates at 120 °C for 72 h. The resultant COF-LZU1-ACOF-1 bilayer membrane exhibited much higher separation selectivity for H_2/CO_2 (24.2), H_2/N_2 (24.2), and H_2/CH_4 (100.2) gas mixtures than the individual COF-LZU1 [H_2/CO_2 (5.99), H_2/N_2 (8.13), and H_2/CH_4 (9.65)] and ACOF-1 [H_2/CO_2 (14.14), H_2/N_2 (21.56), and H_2/CH_4 (24.67)] membranes. The increase of selectivity for the COF-LZU1-ACOF-1 bilayer membrane is attributed to the formed interlaced pores close to the size of gas molecules. The high permeability is ascribed to the thin COF-COF layer of ~1 μm thickness.

Along the same line, Ben and co-workers[91] synthesized a COF–MOF composite membrane on a flat SiO_2 porous substrate. In their study, a continuous and uniform layer of COF-300 was firstly grown on the surface of a SiO_2 disk by condensation of tetra-(4-anilyl)-methane with free aldehyde groups. A MOF crystal layer ($Zn_2(bdc)_2(dabco)$ or ZIF-8) was formed *via* coordination of a zinc cation with terephthalic acid and 1,4-diazabicyclo-[2.2.2]octane (DABCO) or 2-methylimidazole. The resultant [COF-300]-[$Zn_2(bdc)_2(dabco)$] (selectivity: 12.6) and [COF-300]-[ZIF-8] (selectivity: 13.5) composite membranes exhibited much higher separation selectivity for H_2/CO_2 (1 : 1) gas mixtures than the individual COF-300 (6.0), $Zn_2(bdc)_2(dabco)$ (7.0), and ZIF-8 (9.1) membranes due to the formation of chemical bonds between different components (support, COF, MOF) of the membrane, The membrane separation performance surpassed the Robeson upper bound.

3.1.5 Separation of hydrogen isotopes. Deuterium as a stable isotope of hydrogen is a potential energy source for nuclear fusion reactors and is widely used in industrial and scientific research such as nonradioactive isotopic tracing, neutron moderators for heavy-water nuclear reactors, and neutron scattering techniques.[195] Despite the increasing global demand, the natural abundance of deuterium is extremely low (~0.0184% of all hydrogen on earth). Thus, the development of separation technology to enrich deuterium from hydrogen isotopes is in high demand. Unfortunately, separation of hydrogen isotopes is extremely difficult because of their identical shape, size, and thermodynamic properties. Current industrial separation of hydrogen isotopes mainly relies on cryogenic distillation, thermal diffusion, and the Girdler sulfide process.[196] However, these techniques are not easy to operate and are high energy consuming processes.

As a promising alternative separation strategy, kinetic quantum sieving (QS) of isotopes by confinement in a narrow space was first reported in 1995 by Beenakker *et al.*[197] They proposed that if the difference between the aperture diameter and molecular size becomes comparable to the de Broglie

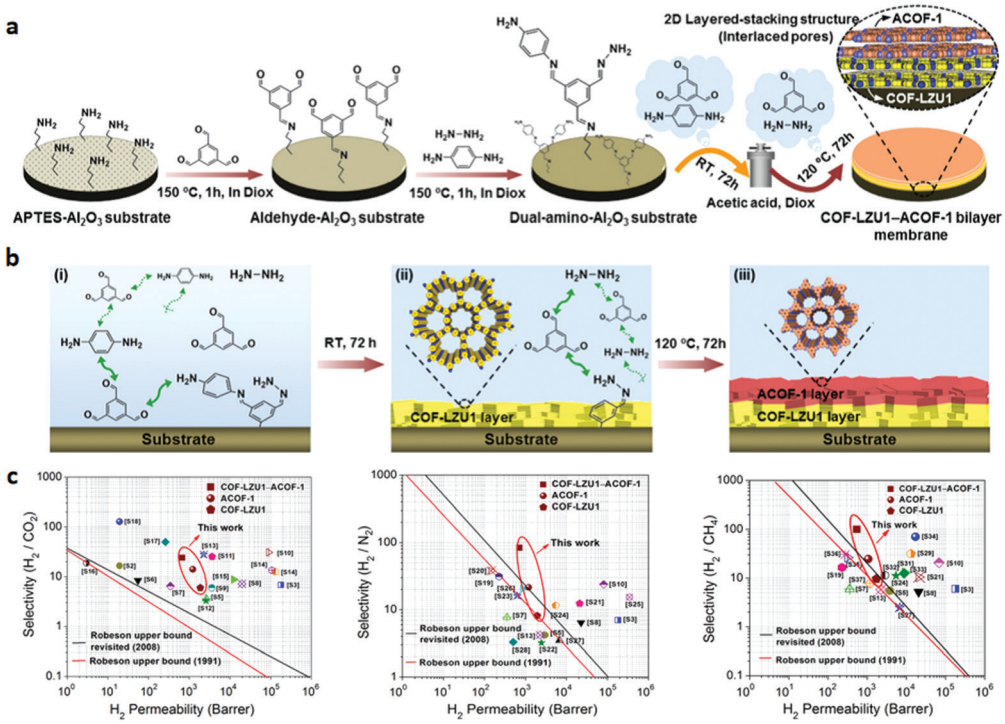

Fig. 17 (a) Schematic representation of the synthesis of a COF-LZU1-ACOF-1 bilayer membrane by a temperature-swing solvothermal approach. (b) Schematic illustration of the reactions and growth of COF–COF membranes. (c) Separation performance of the COF-LZU1-ACOF-1 bilayer membrane under different mixed gases (H_2/CO_2, H_2/N_2, and H_2/CH_4). Reproduced with permission from ref. 194. Copyright 2018, American Chemical Society.

wavelength, the isotope separation in nanopores can be possible due to the quantum effect (the diffusivity of the heavier isotope is faster than that of the lighter one). Since deuterium showed a shorter de Broglie wavelength than hydrogen, the effective molecular size of deuterium is smaller than that of hydrogen. Thus, deuterium exhibited a faster diffusion rate than hydrogen in the porous medium leading to isotope separation.

However, hydrogen isotope separation studies showed high molar ratios only at near zero coverage pressure for rigid porous frameworks.[198,199] Unlike conventional rigid porous frameworks, flexible COFs may exhibit different aperture geometries depending on the exposed temperature and pressure, which may lead to relatively high operating temperature and pressure.[200–202] For example, Hirscher and co-workers[89] studied the hydrogen isotope separation ability by exploiting the flexible nature of pyridine molecules decorated in the pore walls of COF-1. They successfully incorporated pyridine molecules (Py) as flexible gates into the large channel of COF-1 by a Lewis base approach and obtained a close packed structure, Py@COF-1. Notably, Py@COF-1 exhibited a varying degree of hysteresis in the low pressure isotherm with a change in exposure temperature, indicating the existence of a cryogenically flexible aperture. Furthermore, the selectivity for a 1 : 1 D_2/H_2 isotope mixture was significantly higher than those for the molar ratio from pure gas isotherms. This result was mainly ascribed to a quantum isotope effect with cryogenic flexibility (Fig. 18). The S_{D_2/H_2} (the ratio of desorbed amount of D_2 over H_2) increased with pressure and reached its highest value of 9.7 at 26 mbar and 22 K, which

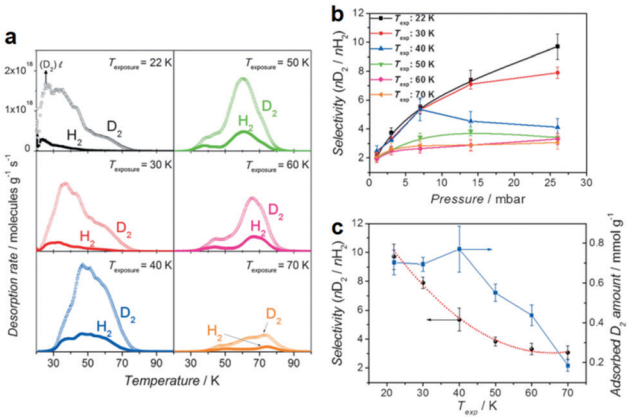

Fig. 18 (a) H_2 and D_2 TDS of 26 mbar (1 : 1 H_2/D_2 mixture) loading on Py@COF-1 with a heating rate of 0.1 K s^{-1}. (b) Equimolar mixture selectivity as a function of loading pressure for different temperatures. (c) T_{exp} dependence of the maximum selectivity and corresponding adsorbed D_2 amount. Reproduced with permission from ref. 89. Copyright 2013, Wiley-VCH.

is far superior to the value of the commercial cryogenic distillation process ($S_{D_2/H_2} \approx 1.5$ at 24 K).

3.2 Liquid phase separation

Liquid separation based on COFs has been used in many fields. According to the practical separation requirements in practical applications, it can be mainly summarized into two categories: water treatment (*e.g.* removal of organic contaminants, heavy

metal from water and seawater desalination) and chromatographic separation (*e.g.* separation of nonchiral compounds or chiral compounds). In this section, the typical liquid separation applications of COFs are highlighted and discussed in detail.

3.2.1 Water treatment. The global environmental crisis and growing human population have put a significant strain on potable water sources available to the society resulting in severe issues such as a lack of water and increased water pollution.[203] In order to address these crises, various advanced separation technologies have been proposed and employed to offer freshwater by purifying seawater or from contaminated water sources.[204–206] Owing to the characteristics described above, COFs have been considered as prominent candidates in the area of water treatment, such as removal of salts, dyes, metal ions and other organics from water.

3.2.1.1 Removal of organic contaminants from water. The Loh group reported a salicylideneaniline-based COF (SA-COF) with chemoselectivity, which displayed reversible proton tautomerism. As a result, the ionic properties of SA-COF were reversibly changed, hence forming the basis for size-dependent separation, charge-selective separation and chemoselective separation. The synthesized SA-COF can not only adsorb molecules with a positive charge under alkaline conditions and exclude them under acidic conditions, but also selectively bind more molecules with aromatic hydroxyl groups than with aromatic amine groups. As a result, the SA-COF was found to show high selectivity for the separation of dye molecules (*e.g.* anthraflavic acid, methylene blue, rhodamine B and chrome azurol S) based on the differences in molecular size and charge. This study demonstrated the utility of COFs as potential candidate materials for molecular separation applications.[207]

Membrane separation has provided many opportunities for water treatment.[208–211] In 2017, the Banerjee group prepared COF membranes based on the COF (Tp–Bpy), which showed excellent performance in permeation of both aprotic and protic solvents such as acetonitrile (339 L m^{-2} h^{-1} bar^{-1}), water (211 L m^{-2} h^{-1} bar^{-1}), ethanol (174 L m^{-2} h^{-1} bar^{-1}), and methanol (108 L m^{-2} h^{-1} bar^{-1}). Moreover, these COF thin films demonstrated remarkable performance in dye-rejection, in which Tp–Bpy displayed rejection values as high as 94% (brilliant blue-G), 80% (congo red), 97% (acid fuchsin) and 98% (rhodamine B).[93] Along the same line, Wang *et al.* synthesized a continuous COF-based membrane using interfacial polymerization with Tp and Pa (Fig. 19). It was found that growing the COF on a polysulfone (PSF) ultrafiltration substrate resulted in the formation of a COF/PSF composite that demonstrated exceptional rejection of congo red (99.5%), but with only a limited water permeability of 50 L m^{-2} h^{-1} bar^{-1}.[212] In 2018, a molecular sieving membrane was fabricated *via* the growth of a continuous 2D imine-linked COF (COF-LZU1) on alumina tubes. Although the pore size of COF-LZU1 was around 1.8 nm, the obtained membrane possessed efficient dye molecule rejection (>90%) when the molecular dimensions of the dye exceeded 1.2 nm. These results could be attributed to the intergrowth of COF-LZU1 or the aggregation of dye molecules in water.[213]

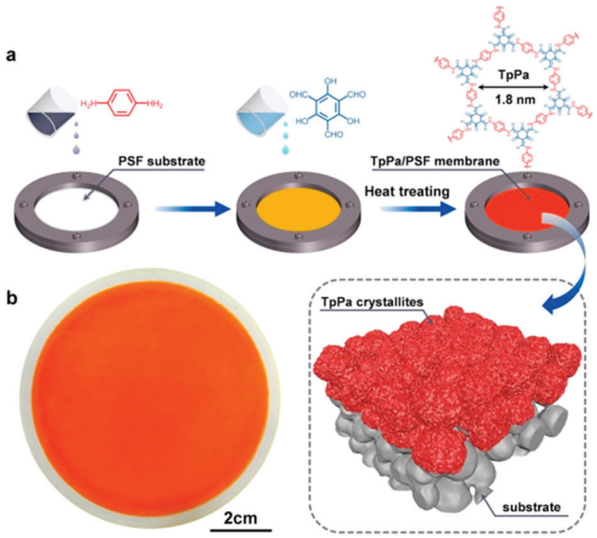

Fig. 19 Schematic illustration of the fabrication process of TpPa/PAF membranes *via* interfacial polymerization. Reproduced with permission from ref. 212 Copyright 2018, Elsevier.

In the same year, the Ma and Li groups synthesized a 2D cationic COF membrane (EB-COF: Br) *via* a bottom-up strategy with interfacial crystallization by combining the cationic monomer (ethidium bromide, EB) *via* the Schiff base reaction (Fig. 20).[214] The fabricated membrane showed outstanding permeation to protic solvents, such as water (546 L m^{-2} h^{-1} bar^{-1}), methanol (1272 L m^{-2} h^{-1} bar^{-1}), and ethanol (564 L m^{-2} h^{-1} bar^{-1}). Owing to the weak dipole interaction between the charged interface of the EB-COF:Br membrane and aprotic solvents, the cationic membrane exhibited higher permeation for aprotic solvents, such as acetone (2640 L m^{-2} h^{-1} bar^{-1}) and acetonitrile (2095 L m^{-2} h^{-1} bar^{-1}). In addition, the EB-COF:Br membrane indicated a highly selective anionic dye molecule removal (methyl orange, 99.6%; fluorescein sodium salt, 99.2%; potassium permanganate, 98.1%) and the separation of ions with differing sizes and charges. These results demonstrated that the separation performance was related to the charges of the COF membrane and the physical size sieving effect.

Next, the Lai group further demonstrated that the decisive molecular size for molecule rejection mainly depended on the smallest projection size of the molecules.[215] In this work, a 2D COF thin film was synthesized using the Langmuir–Blodgett method on an air/water interface. The membrane showed excellent molecular rejection performance for large molecules. For example, small molecules (*e.g.* methyl orange and rhodamine B) were found to pass through the membrane unhindered, while larger molecules (*e.g.* red 80 and PEG) were almost completely rejected. The smallest molecular size of the molecules for successful transport was around 1.3 nm, which was similar to the calculated pore size of the COF membrane. Very recently, Zhang and Wang's groups reported a COF MMM based on hybrid GO/COF-1 nanocomposites and demonstrated good results for water treatment. Owing to the appropriate alignment of adjacent graphene oxide (GO) sheets, the physical size

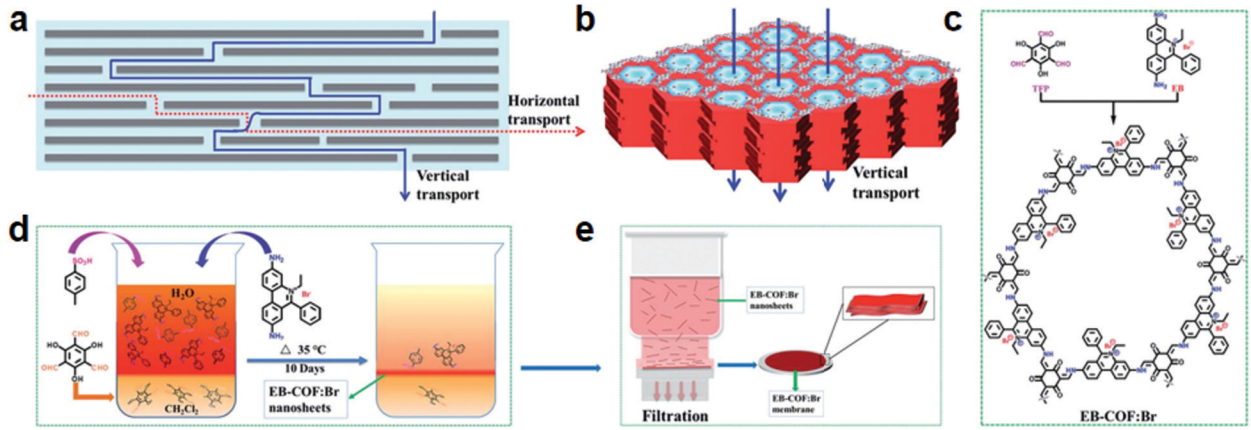

Fig. 20 (a and b) Schematic illustration of the model of the mass transport across 2D graphene oxide sheets and COF membranes; (c–e) the synthesis of the EB-COF:Br membrane. Reproduced with permission from ref. 214. Copyright 2018, Royal Society of Chemistry.

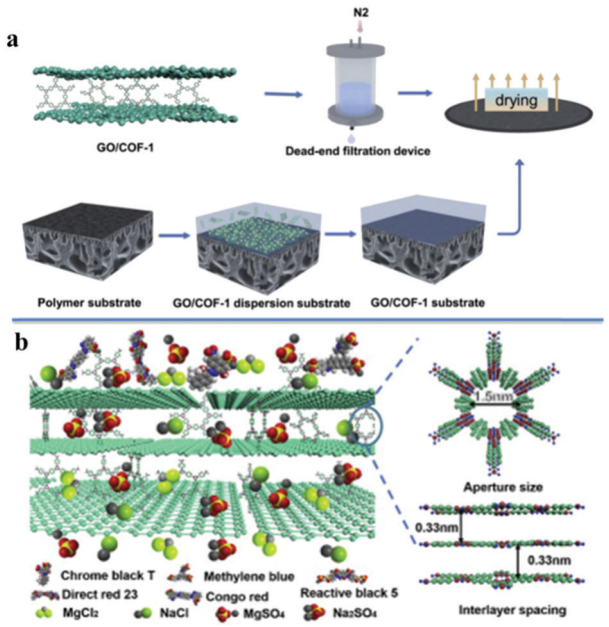

Fig. 21 (a) Schematic illustration of GO/COF-1 membrane fabrication; (b) the molecular sieving mechanism through GO/COF-1 membranes. Reproduced with permission from ref. 216. Copyright 2019, Elsevier.

sieving of COF-1, and the electrostatic interactions between dye molecules and the GO/COF-1 membrane, the constructed membranes exhibited excellent rejection rates for negatively charged dye molecules (Fig. 21).[216]

3.2.1.2 Seawater desalination. As an attractive solution of seawater desalination, reverse osmosis (RO) was widely applied because of its higher energy efficiency.[217–221] During the process of RO, membranes have a significant role in water desalination. COFs have been reported to be fabricated as membranes for desalination performance. In 2017, a series of 2D COFs consisting of Tp and Pa with different functional groups (TpPa-AM_2, -AMC_2NH_2, -OC_3OH, -OC_4H_9, -AMCOOH, -OBn and -AM_3) were computationally designed by the Jiang group.[221] Simulated results for water desalination (Fig. 22) indicated that all

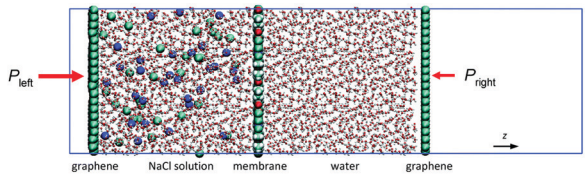

Fig. 22 The simulation system for water desalination through COF membranes (C: cyan; O: red; H: white; Na+: blue; Cl−: cyan). Reproduced with permission from ref. 221. Copyright 2017, Royal Society of Chemistry.

TpPa-X membranes possessed extremely high water permeation values ranging from 1216 to 3375 kg m^{-2} h^{-1} bar^{-1}, which are around three orders of magnitude higher than those of commercial RO membranes (*e.g.* seawater RO, brackish RO and high-flux RO membranes). According to molecular dynamics simulations, the increasing pore size of TpPa-X resulted in an increase in water flux through the TpPa-X membranes which was also significantly affected by the functionality of the membranes. TpPa-X membranes with hydrophilic functional groups exhibited higher water flux than the membranes with hydrophobic functionalities and similar pore size, which is attributed to the preferential interaction of water with hydrophilic pore walls. Furthermore, the membranes exhibited a high salt rejection of $>98\%$, with the exception of TpPa-AMCOOH with a comparatively lower 95.8%. These results revealed that the salt rejection and water flux are associated with the aperture size difference, hydrophobicity and hydrophilicity of COFs. According to the simulation results reported by the Jiang group, these TpPa-X COFs demonstrated the highest water flux when the 2D COFs were present as monolayers.

However, the fabrication of COF monolayers is far from being a trivial procedure under practical conditions. Therefore, the Wang and Wei groups studied how multilayer stacking influenced water permeation and revealed an increase in ion rejection with increasing layer numbers and a subsequent decrease in water permeation. The hydrogen bonds and the interaction between oxygen and nitrogen atoms in water molecules and pore walls offered the resistance in the water transport process. Moreover, due to differences in the effective

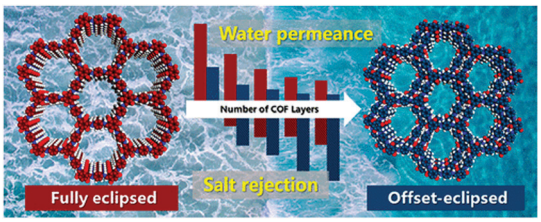

Fig. 23 The transport behaviour of water and salt ions through multi-layered COFs. Reproduced with permission from ref. 222. Copyright 2019, American Chemical Society.

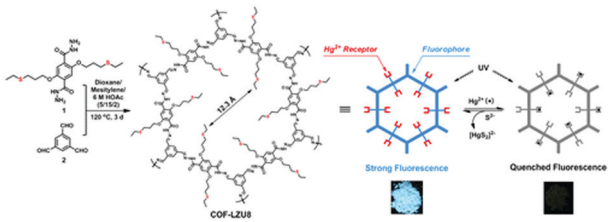

Fig. 24 Schematic illustration of the synthesis route of COF-LZU8 and its application for Hg^{2+} detection and removal. Reproduced with permission from ref. 224. Copyright 2016, American Chemical Society.

pore diameters between offset-eclipsed and fully eclipsed multi-layered COFs, the permselectivity of multi-layered COFs may be significantly altered. In the case of the fully eclipsed multi-layered TpPa-1 COF, with an effective pore size of 1.58 nm, when modelled with 25 monolayers the water permeation was found to be 3201 L m^{-2} h^{-1} bar^{-1} while $MgCl_2$ rejection was only 42%. However, in a marginally offset-eclipsed structure, with an effective pore diameter of 0.89 nm, the 25 COF monolayers offered 100% rejection of $MgCl_2$ with water permeation falling to 1118 L m^{-2} h^{-1} bar^{-1}. These results demonstrate the importance of layer thickness and alignment of COF layers for nanofiltration performance (Fig. 23).[222] Charged COF layers have also been identified for their utility in desalination. In 2018, Kuehl and co-workers synthesized a series of 2D COFs with ordered nano-sized pores that can be readily functionalized. When functionalised with 12 ionizable carboxylic acid groups, a COF with pore size of 2.8 nm was synthesized and used to fabricate membranes that showed both high water flux (~2260 L m^{-2} h^{-1} bar^{-1}) and highly size selective cation rejection, with a nearly complete rejection of Oct_4N (nearly complete rejection of Oct_4N radius with size of 1.09 nm and dodecyl with size of 1.51 nm).[223]

3.2.1.3 Removal of toxic ions. COFs have also been applied in the removal of toxic ions from the environment. The major challenge in this field is the design of COFs with plentiful accessible chelating sites, to achieve rapid uptake as well as high capacity for toxic ions. The first reported example of this field was a thioether-functionalized hydrazine-linked COF (COF-LZU8) for the detection and removal of toxic heavy metals such as Hg^{2+} by Wang's group.[224] Owing to the distinct π-donor character and soft nucleophilic nature of sulfur, COF-LZU8 is an efficient ionophoric receptor for Hg^{2+}. The real-time fluorescence response and the color change of COF-LZU8 under a UV lamp demonstrated good sensitivity toward Hg^{2+} detection. Moreover, due to the 2D eclipsed structure (with a narrow channel of ~1.2 nm promoting Hg^{2+} and sulfur contact), COF-LZU8 showed affinity for Hg^{2+} removal even under extremely high dilution (Fig. 24). Subsequently, the Jiang group designed and synthesized an extremely stable imine-linked COF, and introduced methyl sulfide units onto the pore walls of the 2D COF (TAPB-BMTTPA-COF).[225] Due to the high accessibility of methyl sulfide groups that offered the well-established Hg^{2+}-thioether ligation chemistry, the TAPB-BMTTPA-COF displayed higher Hg^{2+} removal capacity (734 mg g^{-1}) than most of the normal porous materials, such as Zr-DMBD MOF (197 mg g^{-1}),[226] porous carbon (518 mg g^{-1}),[227] mesoporous silica (600 mg g^{-1}),[228] and chalcogel-1 (645 mg g^{-1}).[229] In particular, the TAPB-BNTTPA-COF showed more than 3-fold Hg^{2+} removal capacity compared to COF-LZU8 (236 mg g^{-1}) reported by the Wang group. In addition, the distribution coefficient (K_d) of the COF was calculated to be 7.82×10^5 mL g^{-1}, which was comparable to those of the benchmark materials, such as Zr-DMBD (9.99×10^5 mL g^{-1})[226] and porous carbon (6.82×10^5 mL g^{-1}).[227] More importantly, the TAPB-BMTTPA-COF could retain its structure stability under harsh conditions for practical use. These results demonstrated the huge potential of the TAPB-BMTTPA-COF for diverse Hg pollution issues.

In 2017, our team synthesized a novel vinyl-functionalized mesoporous COF (COF-V) which was modified with a 1,2-ethanedithiol group to obtain a sulfur functionalized COF (COF-S-SH). Owing to the strong binding affinity of the densely-packed sulfur chelating groups, the COF exhibited higher performance in mercury removal from air and aqueous solutions (with an Hg capacity of 863 mg g^{-1} and Hg^{2+} capacity of 1350 mg g^{-1}) than the TAPB-BMTTPA-COF reported by the Jiang group. More importantly, the COF-S-SH showed a superhigh distribution coefficient value (K_d) of 2.3×10^9 mL g^{-1}, that allowed it to reduce the Hg^{2+} concentration from 5 ppm to lower than 0.1 ppb rapidly (below the 2 ppb acceptable limit for drinking water).[230] An amidoxime functionalized 2D COF (COF-TpAb-AO) was also synthesized as highly efficient sorbents for uranium sequestration by our group.[231] This study showed that the COF-TpAb-AO was capable of extracting uranium from various contaminated waters. The efficient performance was mainly because of the open 1D channels that exhibited exceptional accessibility from the chelating groups. Moreover, the chelating groups were tightly coordinated with each other due to the dense packing of extended polygons in the 2D COF making chelating groups in adjacent layers parallel to each other. Therefore, compared with the amorphous POP analogue, the COF-TpAb-AO displayed higher uranium adsorption capacities, kinetics, and affinities (Fig. 25). In particular, the COF-TpAb-AO could reduce uranium in various contaminated waters from 1 ppm to less than 0.1 ppb (the maximum acceptable concentration limit was 30 ppb defined by the US Environmental Protection Agency). Additionally, the COF-TpAb-AO showed a super high uranium uptake capacity of 127 mg g^{-1} from spiked seawater.

More recently, the Yan group reported a cationic covalent organic nanosheet (iCON) for efficient adsorption of ReO_4^-

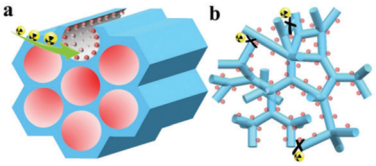

Fig. 25 (a) Chelating groups in the uniform pores of the COF-TpDb-AO; (b) chelating groups in amorphous porous organic polymers. Reproduced with permission from ref. 231. Copyright 2018, Wiley-VCH.

(the nonradioactive surrogate of TcO_4^-). iCON displayed fast exchange kinetics toward ReO_4^-, with a high adsorption capacity of 437 mg g^{-1} as well as an excellent distribution coefficient of 5.0×10^5. This was attributed to the combination of cationic guanidine-based monomers with hydroxyl anchored neutral edge units, and the loosely bonded chloride ions present in iCON (making it easy to achieve anion exchange between Cl^- and ReO_4^-).[232] These reports presented here demonstrate the exceptional potential of COFs for high-efficiency toxic ion removal.

3.2.2 Chromatographic separation of small organic molecules. Chromatographic separation is the most universally used precision analysis and separation method in diverse research fields such as chemical engineering, pharmaceutical science, and environmental detection.[233–235] The key of every chromatographic system lies in the stationary phase which determines the separation efficiency and capability.[236] The separation performance of the stationary phase mainly involves noncovalent interactions, such as hydrophilic, hydrophobic, size-exclusion or even chiral-specific interactions, between the stationary phase and analytes. Improvements in chromatographic separation are therefore dependent on the discovery of new permeable materials with specific interactions with a variety of chemicals.[237–240]

High surface area, tuneable pore sizes, good stability and highly customizable pore chemistry render COFs highly desirable materials for stationary phases. Additionally, due to the hydrophobic interaction, π···π interaction and electron-donor–acceptor interaction between COFs and analytes, especially the size selectivity of porous COF structures, COFs further show great application prospects as stationary phases for chromatographic separation.

3.2.2.1 Chromatographic separation of nonchiral compounds. An increasing number of COFs have been investigated as stationary phases in chromatographic separation systems, including high-performance liquid chromatography (HPLC), gas chromatography (GC) and capillary electrochromatography (CEC). Examples of COFs and their applications in chromatographic separation are summarized in Table 2.

In 2015, Yan and co-workers for the first time reported a spherical TpBD COF stationary phase prepared as a coated capillary column *via* a facile room-temperature solution-phase approach for application in high-resolution GC (Fig. 26). Owing to the relatively different van der Waals interactions between the hydrophobic aromatic frameworks of TpBD and important industrial analytes such as linear alkanes, the TpBD coated capillary offered high-resolution separation for these analytes. Additionally, separation within the column was also attributed to π···π interactions and hydrogen bonding. For instance, the separation of positional isomers α-pinene and β-pinene mainly relies on differences in π···π interactions between analytes and the TpBD COF. The separation of alcohols on the capillary can be attributed to hydrogen bonding interactions between the amino or carbonyl groups of TpBD and the hydroxyl groups of alcohols.[92]

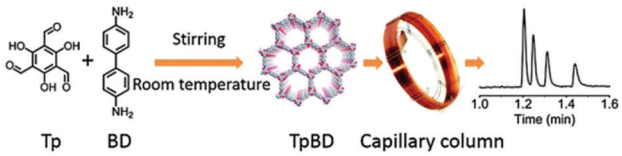

Fig. 26 Schematic illustration of room-temperature synthesis of TpBD for high-resolution GC. Reproduced with permission from ref. 92. Copyright 2015, Royal Society of Chemistry.

Table 2 The COFs used as stationary phases for chromatographic separations

COFs	Linkages	SA_{BET} [m^2g^{-1}]	Pore width [nm]	Pore volume [cm^3g^{-1}]	Analytes	Ref.
TpBD	Imine	885	2.3	—	Alkanes/cyclohexane and benzene *etc.*	92
COF-LZU1	Imine	—	Layer distance 0.37	—	Alkylbenzenes/anilines/polyaromatic hydrocarbons	241
TpPa-MA	Imine	317	1.5	—	Polycyclic aromatic hydrocarbons/acidic/basic compounds *etc.*	95
COF-5	Boronate ester	—	2.7	—	Neutral, acidic, basic analytes	242
COF-SNW-1	C═C linkage	—	—	—	SAs, cephalosporins, amino acid and parabens	245
TpPa-1	Imine	—	—	—	Neutral analytes, NSAIDs and food additives	244
BtaMth COF	Hydrazone	723	1.41	0.46	Positional isomers	247
Salen-COF 1	Schiff-base	666	0.78	0.43	C8 alkyl-aromatic isomers	250
Salen-COF 2		701	0.78	0.38		
Zn(salen)-COF 1-Zn		460	0.78	0.31		
Zn(salen)-COF 2-Zn		535	0.78	0.22		
CTpPa-1	Imine	146	1.3	0.48	(±)-1-Phenylethanol, (±)-1-phenyl-1-propanol,	257
CTpPa-2	Imine	104	1.2	—	(±)-limonene and (±)-methyl lactate, *etc.*	
CTpBD	Imine	317	1.8	—		
CCOF 5	Imine	655	0.62/0.74	0.51	Racemic alcohols	258
CCOF 6	Amide	613	0.59/0.74	0.42		
COF 1	Amide	714	3.7	—	Amino acids and drugs	259

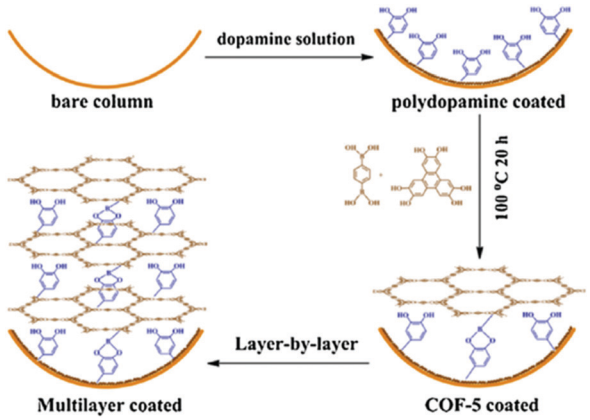

Fig. 27 The growth of multilayer COF-5 on the inner wall of a polydopamine-coated capillary. Reproduced with permission from ref. 242. Copyright 2016, Elsevier.

In 2016, COF-LZU1 was used as the stationary phase in open-tubular capillary electrochromatography (OT-CEC) for the first time by Niu and co-workers. The imine-linked COF-LZU1 was fabricated and coated on a capillary column by covalent linkage. The column demonstrated excellent separation performance for several model analytes (*e.g.* alkylbenzenes, polyaromatic hydrocarbons (PAHs) and anilines) as a result of the size selectivity of the porous COF structure, and the hydrophobic interactions between the organic building blocks of COF-LZU1 and the model analytes.[241] Subsequently, the Chen group prepared a COF-5 coated capillary column using a polydopamine (PDA) modification strategy for OT-CEC (Fig. 27). The COF-5 coated column showed high separation efficiency, outstanding stability, repeatability and reproducibility in the separation of neutral, acidic and basic analytes. By contrast, the capillary solely coated with polydopamine (PDA@capillary) exhibited no separation capability. These results demonstrated the increased interactions (such as π···π, hydrophobicity, dipole···dipole) between model analytes and the COF-5-coated column, contributing to the high efficiency of separation.[242] The group then prepared a capillary column coated with COF-LZU1 *via* an *in situ* growth method. An aldehyde-functionalized capillary was obtained by treatment with 3-aminopropyltriethoxysilane (APTES) and glutaraldehyde, which was subsequently used as a cross support for COF-LZU1 growth. Compared with the aldehyde functionalized capillary, the COF-LZU1-modified column showed remarkable improvement for separation of neutral analytes, amino acids and nonsteroidal anti-inflammatory drugs (NSAIDs). These results further demonstrated that the interactions between COF-LZU1 and the analytes play a vital role in the separation.[243] In 2018, a COF-TpPa-1 modified capillary column was also constructed by the Chen group *via* an *in situ* growth method. The obtained column showed good resolution for the separation of neutral analytes, NSAIDs and food additives in open-tubular CEC mode.[244] Similarly, a Schiff base network (SNW-1) was covalently attached within a capillary column by Ye *et al.* The obtained SNW-1-coated capillary column was successfully applied for the separation of sulfonamides (SAs), cephalosporins, amino acids and parabens in OT-CEC mode. Among them, the retention factors for SAs and amino acids were correlated with their pKa values. The successful separation of cephalosporins can be attributed to the intermolecular hydrogen bonds and π···π stacking interactions between SNW-1 and cephalosporins. In addition, the SNW-1 column showed good resolution for four parabens as a result of differences in molecular sizes and steric effects of the analytes.[245] All these results demonstrated the significant potential of COFs for application in chromatographic separation.

Compared to the COF-based stationary phases for GC and OT-CEC, COF-based LC stationary phases have been relatively less reported. The reasons for this may include the fact that traditional methods for COF synthesis often result in sub-micrometer sized particles which, when directly packed into a column, would result in high column pressure and low efficiency. In 2017, the Yan and Yang groups for the first time fabricated a methacrylate-bonded COF poly(TpPa-methacrylic anhydride-*co*-ethylene dimethacrylate) (poly(TpPa-MA-*co*-EDMA)) monolithic column for high-performance liquid chromatography (Fig. 28). Compared with the poly(MMA-*co*-EDMA) monolithic column in the absence of COFs, the obtained COF-bonded monolithic column showed high efficiency and precision for the separation of PAHs, phenols, anilines, NSAIDs and benzothiophenes. These benefits were attributed to improved transfer properties between the analytes and stationary phase, increased permeability and lower back pressure. Addition of the aromatic TpPa-MA to the monolith is thought to have increased the hydrophobicity of the column, hence increasing the performance for HPLC separation.[95]

In the same year, monodispersed COF@SiO_2 microspheres with uniform and tuneable TpBD COF shells were also synthesized *via* an *in situ* growth strategy, and used as the stationary phase for HPLC by the same group. The TpBD@SiO_2 packed columns also displayed high resolution for the separation of small molecules, such as toluene and ethylbenzene, PAHs, *p*-cresol and *p*-chlorophenol, and so on.[246] In another example, the Zhang and Cai groups constructed a new hydrazine-linked chiral BtaMth COF *via* a bottom-up strategy which was developed into a BtaMth@SiO_2 stationary phase in a one-pot synthetic reaction. The prepared BtaMth@SiO_2 HPLC column exhibited high resolution performance for the separation of positional

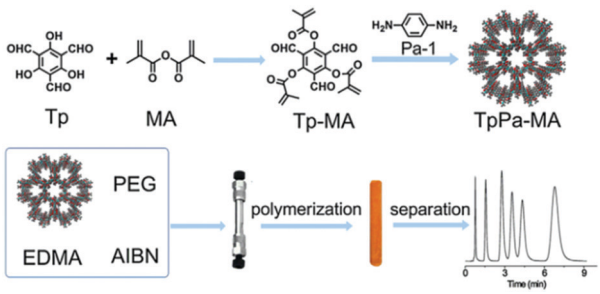

Fig. 28 Schematic illustration of the fabrication of the poly(TaPa-MA-*co*-EDMA) monolith for HPLC. Reproduced with permission from ref. 95. Copyright 2017, Elsevier.

isomers and *cis–trans* isomers, including nitrotoluenes, nitrochlorobenzenes, beta-cypermethrin and metconazole. In the separation of nitrotoluene positional isomers (*e.g. o*-nitrotoluene, *p*-nitrotoluene and *m*-nitrotoluene), the hydrophobic interaction between isomers and the BtaMth COF was thought to significantly affect the separation efficiency. In addition, the separation of *cis–trans* isomers (*e.g. cis* beta-cypermethrin/*trans* beta-cypermethrin and *cis* metconazole/*trans* metconazole) was related to the length-to-width ratio of the analytes.[247]

Similarly, covalent triazine-based framework (CTF) decorating silica gel microspheres were fabricated *via* the growth of CTFs onto the supporting silica spheres by Zhang *et al.*[248] The obtained CTF–SiO_2 stationary phase packed HPLC column exhibited excellent separation efficiency for a large variety of molecules, such as mono-substituted benzenes, PAHs and polar compounds. In 2019, Chen and co-workers prepared a novel multimode COF-300@SiO_2 liquid chromatography stationary phase *via* an *in situ* growth strategy.[249] The separation performance and retention mechanisms of the COF-300@SiO_2 column were further investigated in reverse phase (RP) and normal phase (NP) modes by selecting neutral and polar molecules, such as benzene, naphthalene, phenanthrene, and pyrene, as analytes. In the NP mode, only neutral molecules could be partly or completely separated due to π···π interactions. However, all the neutral and polar analytes can be separated efficiently in the RP mode due to the π···π interactions, electron-donor–acceptor interactions, hydrophobic interactions and the size selectivity of the COF structure. Additionally, owing to the amino groups in COF-300, the analytes including nucleosides, nucleobases and alkaloids were able to be separated on the column in the hydrophilic phase mode. Recently, the Cui group synthesized four isostructural Schiff-based 3D COFs (salen- and Zn(salen)-based COFs), which were shown to be effective as HPLC stationary phases for the separation of xylene isomers and ethylbenzene (EB) (Fig. 29). In contrast, the Zn(salen)-based COFs were found to be ineffective in this separation. These results indicated that the uncoordinated polar salen units in COF 1 and 2 offered the major specific isomer identification and shape-selective separation for analytes.[250] These works significantly extend the application of COFs in the field of chromatographic separation.

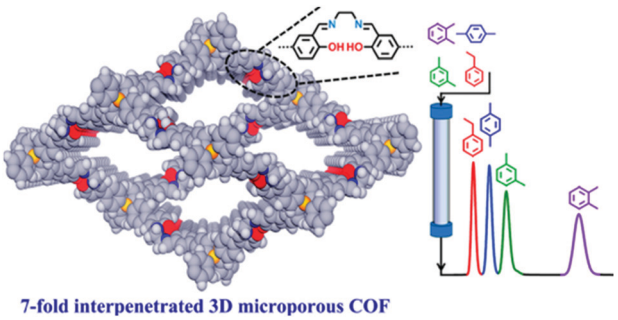

Fig. 29 Schematic illustration of microporous 3D COFs and their use as stationary phases for HPLC. Reproduced with permission from ref. 250. Copyright 2018, American Chemical Society.

3.2.2.2 Chromatographic separation of chiral compounds. Chiral resolution is a crucial technique for the production of chemicals and biologically active compounds due to the fact that the biological behavior, metabolism, and toxicity of pure enantiomers may often differ significantly.[251–253] These studies have aroused continuous interest in the development of new materials and approaches for the efficient separation of enantiomers.

Recently, chiral porous framework materials have shown great promise in diverse fields such as separation, recognition and catalysis.[254–256] As a result of the distinct features, chiral COFs are highly desirable for application in chiral separation and prompt their application in a variety of chromatographic separation techniques such as high resolution GC and HPLC. The pioneering work using COFs in chiral separation was performed by the Yan group in 2016.[257] A series of chiral COFs, CTpPa-1, CTpPa-2 and CTpBD, were synthesized *via* a bottom-up strategy using the chiral organic monomer CTp ((+)-diacetyl-L-tartaric anhydride functionalized 1,3,5-triformylphloroglucinol). Chiral COF-bound capillary columns based on these chiral COFs were fabricated *via* an *in situ* growth approach for chiral gas chromatographic separation. The modified chiral capillary columns showed high resolution for the separation of enantiomers, such as (±)-1-phenylethanol, (±)-1-phenyl-1-propanol, (±)-limonene, demonstrating excellent repeatability and reproducibility. In addition, the influence of the chiral microenvironment as a result of the chiral COF of capillary columns was studied using a column functionalized with the (+)-diacetyl-L-tartaric anhydride monomer. It was found that the monomer-bound column displayed no chiral separation performance compared with the chiral COF-bound column. These results revealed that the abundant interactions offered by the chiral COF and the analytes, including hydrogen-bonding, π···π interactions and size-exclusion, were essential to the chiral resolution. In general, the unique COF structures, combined with the chirality of (+)-diacetyl-L-tartaric anhydride, provided the essential chiral microenvironment and strong column–analyte interactions for the chromatographic separation. This study promoted the continued development of chiral COFs for applications in chiral separation. Subsequently, Han and co-workers synthesized the first 3D chiral COF (CCOF 5) by the imine condensation of chiral tetraaldehyde and tetrahedral tetraamine building blocks.[258] An isostructural amide-linked CCOF 6 was obtained *via* the post-synthetic oxidation of the CCOF 5 framework. Both CCOF 5 and 6 were used as CSPs in HPLC for the separation of racemic alcohols, in which the CCOF 6 packed column was found to be effective in the separation of various racemates including 1-phenyl-2-propanol, 1-phenyl-1-pentanol, 1-phenyl-1-propanol and 1-(4-bromophenyl)-ethanol, with high selectivity factors (α) and chromatographic resolution (R_s) (α/R_s = 1.29/1.78, 1.21/1.58, 1.33/2.47 and 1.24/1.54, respectively) (Fig. 30). However, the column packed with CCOF 5 afforded only baseline resolution of the racemic 1-phenyl-2-propanol (α = 1.19 and R_s = 1.52). The superior resolution performance of CCOF 6 highlights the importance of pore chemistry in the effective separation of analytes, with the

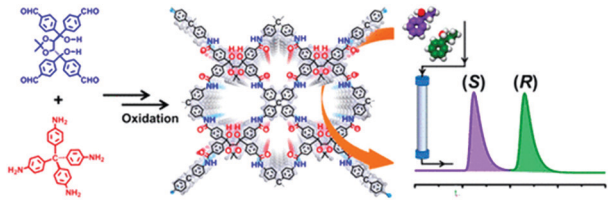

Fig. 30 Schematic illustrations for the synthesis of 3D chiral COFs and their use as CSPs for HPLC. Reproduced with permission from ref. 258. Copyright 2019, American Chemical Society.

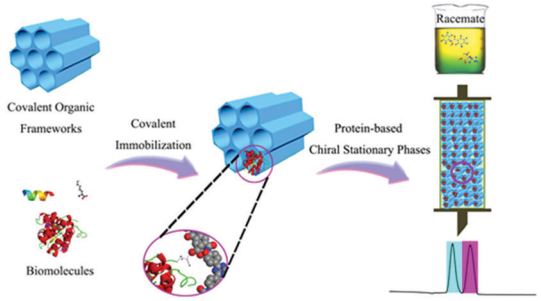

Fig. 31 Illustration of fabricating the biomolecules ⊂ COF 1 stationary phase for chiral separation. Reproduced with permission from ref. 259. Copyright 2018, Wiley-VCH.

increased hydrogen bonding of the amide groups in CCOF 6 offering increased selectivity compared with the imine groups of CCOF 5.

In 2018, our group developed a new strategy to introduce chirality into the achiral COF-1 *via* the covalent anchoring of chiral biomolecules, such as lysozyme, peptide and L-lysine, onto the channel wall (Fig. 31).[259] The obtained biomolecules ⊂ COF composites were found to inherit both the specific interactions and chirality of the anchored biomolecules, while also retaining the crystallinity, stability and porosity of the initial COF. The composites were used as CSPs in both RP and NP HPLC resulting in exceptional chiral separation efficiency for various racemates including DL-threonine, DL-tryptophan, ofloxacin, and metoprolol. Additionally, the studied CSPs exhibited good reproducibility and reusability due to the protection effect provided by COF 1. Since the synthesis of COFs with chirality originating from the building units is very challenging and costly, the strategy created by us showed more potential for practical applications considering the relatively low cost of achiral COFs and biomolecules.

4. Conclusions and outlook

In the past few years, COFs have emerged as one of the ideal candidate materials for advanced separation applications, due to their high porosity, large surface areas, well-defined pore structures, tunable pore sizes, adjustable surface properties and excellent stability. Although remarkable advances have been achieved in COF-based separations, some crucial challenges still remain to be addressed, which also provide great opportunities for researchers in this field.

To date, one of the biggest challenges in COF synthesis has been the construction of ultra-microporous (<0.6 nm)[260] COF materials to realize ultrafast and highly selective molecular sieving. Although changing the length of building units has been employed to modulate pores with different shapes and sizes from mesopores to micropores, COFs with pore sizes less than 1 nm were still rarely obtained due to the size limitation of building units. In this regard, there have been three feasible approaches aimed at addressing this issue: (a) constructing A–B stacking 2D COFs, (b) preparing 3D interpenetrated COFs, and (c) pore surface engineering by anchoring side groups on COF inner walls. Such strategies may yet achieve progress in breaking the size limitations on COFs to yield highly stable ultra-microporous COFs.

Over the past decade, increasing attention has also been paid on developing continuous COF-based membranes for gas and liquid separation, and great success have been achieved using strategies such as layer-to-layer stacking, *in situ* growth and interfacial polymerization. However, the major bottleneck may come from the poor mechanical performance and the large pore size of COF membranes, which significantly restrict the practical applications of COF membranes during pressure-driven filtration processes. Developing new synthetic strategies to fabricate high performance COF membranes is highly desired. Very recently, the reported freestanding polyCOF membranes have injected new vitality into the preparation of continuous COF membranes with outstanding mechanical properties and superior separation performance. In order to expand the scope of the polyCOF strategy, more efforts should be put on designing new types of polymers to serve as building units of polyCOFs. Moreover, 3D COF membranes are relatively less studied than 2D COF membranes. Further studies can be focused on 3D COFs because the pore size of 3D COFs is often small due to the existence of structural interpenetration.

Finally, the practical applications of COF-based membranes in industrial manufacturing remains a challenge. One of the main reasons is that studies on the long-term stability of COF-based membranes under realistic separation conditions are still very limited. At present, research in this field mainly focuses on gas separation and mild liquid separation, including water treatment and organic solvent nanofiltration. Explorations on the long-term stability of COF membranes in acidic/basic environments or complicated organic solvent systems are urgently demanded.

In summary, we provided a comprehensive overview of the research progress in separation applications of COF materials, including gas separation, water treatment, chiral separation, organic solvent nanofiltration, *etc.* We believe that along with the dramatic development of synthetic chemistry, materials chemistry and chemical engineering, this research area will witness a rapid growth proceeding to practical applications in the near future. We hope this work will provide guidance for the design and synthesis of functional COFs for the development of advanced separation protocols, and inspire innovations in this emerging field.

Abbreviations

COFs	Covalent organic frameworks
MOFs	Metal–organic frameworks
HCPs	Hyper-cross-linked polymers
CMPs	Conjugated microporous polymers
PAFs	Porous aromatic frameworks
1D	One-dimensional
2D	Two-dimensional
3D	Three-dimensional
Tp	1,3,5-Triformylphloroglucinol
BD	Benzidine
TpBD	A COF synthesized from 1,3,5-triformylphloroglucinol and benzidine
MMMs	Mixed matrix membranes
CNFs	Cellulose nanofibers
TGCl	Triaminoguanidinium chloride
PAN	Polyacrylonitrile
HTTP	2,3,6,7,10,11-Hexahydroxytriphenylene
SLG	Single-layer graphene
PTSA	*p*-Toluene sulfonic acid
PolyCOFs	Polymer–covalent organic frameworks
TB/TFB	1,3,5-Triformylbenzene
DTH	2,5-Diethoxyterephthalohydrazide
Pa-1	*p*-Phenylenediamine
IAST	Ideal adsorbed solution theory
COF	Nitrogen-rich COF
ACOF	Azine-linked COF
TAPB	1,3,5-Tris(4-aminophenyl)benzene
BMTTPA	2,5-Bis(methylthio)terephthalaldehyde
Q_{st}	Isosteric heats of adsorption
SA-COF	Salicylideneaniline-based COF
Bpy	2,2′-bipyridine-5,5′-diamine
PSF	Polysulfone
EB	Ethidium bromide
GO	Graphene oxide
RO	Reverse osmosis
COF-V	Vinyl-functionalized COF
iCON	Cationic covalent organic nanosheet
HPLC	High-performance liquid chromatography
GC	Gas chromatography
CEC	Capillary electrochromatography
OT-CEC	Open-tubular capillary electrochromatography
PAHs	Polyaromatic hydrocarbons
PDA	Polydopamine
APTES	3-Aminopropyltriethoxysilane
NSAIDs	Nonsteroidal anti-inflammatory drugs
SAs	Sulfonamides
SNW-1	Schiff base network-1
MA	Methacrylic anhydride
poly(TpPa-MA-*co*-EDMA)	Poly(TpPa-methacrylic anhydride co-ethylene dimethacrylate)
Mth	(*S*)-2,5-Bis(2-methylbutoxy)terephthalohydrazide
CTFs	Covalent triazine-based frameworks
RP	Reverse phase
NP	Normal phase
CSP	Chiral stationary phase
CTp	Chiral (+)-diacetyl-L-tartaric anhydride functionalized Tp
CCOF	Chiral COF

Conflicts of interest

The authors declare no competing interest.

Acknowledgements

The authors acknowledge the financial support from the National Natural Science Foundation of China (21971126, 21871153 and 31800793), Tianjin Natural Science Foundation of China (18JCZDJC37300), 111 Project (B12015) and the National Key Research and Development Program of China (2018YFA0901800). Partial support from the US National Science Foundation (CBET-1706025) and the University of South Florida is also acknowledged.

References

1 C. J. King, *Separation Progress*, McGraw-Hill, New York, 2nd edn, 1980.
2 B. L. Karger, R. L. Snyder and H. Horvath, *An Introduction to Separation Science*, Wiley, New York, 1973.
3 J.-i. Yoshida and K. Itami, *Chem. Rev.*, 2002, **102**, 3693–3716.
4 P. Vandezande, L. E. Gevers and I. F. Vankelecom, *Chem. Soc. Rev.*, 2008, **37**, 365–405.
5 P. Pandey and R. S. Chauhan, *Prog. Polym. Sci.*, 2001, **26**, 853–893.
6 M. Iranmanesh and J. Hulliger, *Chem. Soc. Rev.*, 2017, **46**, 5925–5934.
7 Z. Zhang, L. Wen and L. Jiang, *Chem. Soc. Rev.*, 2018, **47**, 322–356.
8 D. S. Sholl and R. P. Lively, *Nature*, 2016, **532**, 435–437.
9 J. W. Yoon, H. Chang, S.-J. Lee, Y. K. Hwang, D.-Y. Hong, S.-K. Lee, J. S. Lee, S. Jang, T.-U. Yoon, K. Kwac, Y. Jung, R. S. Pillai, F. Faucher, A. Vimont, M. Daturi, G. Férey, C. Serre, G. Maurin, Y.-S. Bae and J.-S. Chang, *Nat. Mater.*, 2016, **16**, 526.
10 J.-R. Li, R. J. Kuppler and H.-C. Zhou, *Chem. Soc. Rev.*, 2009, **38**, 1477–1504.
11 C. Z. Liang, T.-S. Chung and J.-Y. Lai, *Prog. Polym. Sci.*, 2019, **97**, 101141.
12 S. Basu, A. L. Khan, A. Cano-Odena, C. Liu and I. F. J. Vankelecom, *Chem. Soc. Rev.*, 2010, **39**, 750–768.
13 S. Sircar, T. C. Golden and M. B. Rao, *Carbon*, 1996, **34**, 1–12.
14 A. Dąbrowski, P. Podkościelny, Z. Hubicki and M. Barczak, *Chemosphere*, 2005, **58**, 1049–1070.
15 E. Erdem, N. Karapinar and R. Donat, *J. Colloid Interface Sci.*, 2004, **280**, 309–314.
16 G. E. Boyd, A. W. Adamson and L. S. Myers, *J. Am. Chem. Soc.*, 1947, **69**, 2836–2848.

17 L. Tan and B. Tan, *Chem. Soc. Rev.*, 2017, **46**, 3322–3356.
18 V. A. Davankov, S. V. Rogozhin and M. P. Tsyurupa, *US Pat.*, 3729457, 1971.
19 J.-X. Jiang, F. Su, A. Trewin, C. D. Wood, N. L. Campbell, H. Niu, C. Dickinson, A. Y. Ganin, M. J. Rosseinsky, Y. Z. Khimyak and A. I. Cooper, *Angew. Chem., Int. Ed.*, 2007, **46**, 8574–8578.
20 R. Dawson, A. I. Cooper and D. J. Adams, *Prog. Polym. Sci.*, 2012, **37**, 530–563.
21 A. I. Cooper, *Adv. Mater.*, 2009, **21**, 1291–1295.
22 T. Ben, C. Pei, D. Zhang, J. Xu, F. Deng, X. Jing and S. Qiu, *Energy Environ. Sci.*, 2011, **4**, 3991–3999.
23 T. Ben, H. Ren, S. Ma, D. Cao, J. Lan, X. Jing, W. Wang, J. Xu, F. Deng, J. M. Simmons, S. Qiu and G. Zhu, *Angew. Chem., Int. Ed.*, 2009, **48**, 9457–9460.
24 S. L. James, *Chem. Soc. Rev.*, 2003, **32**, 276–288.
25 O. M. Yaghi, G. M. Li and H. L. Li, *Nature*, 1995, **378**, 703.
26 S. Subramanian and M. J. Zaworotko, *Angew. Chem., Int. Ed. Engl.*, 1995, **34**, 2127.
27 G. B. Gardner, D. Venkataraman, J. S. Moore and S. Lee, *Nature*, 1995, **374**, 792.
28 B. F. Hoskins and R. Robson, *J. Am. Chem. Soc.*, 1989, **111**, 5962.
29 J. Y. Kim, H. Oh and H. R. Moon, *Adv. Mater.*, 2019, **31**, e1805293.
30 X. Zhao, Y. Wang, D. S. Li, X. Bu and P. Feng, *Adv. Mater.*, 2018, **30**, e1705189.
31 J.-R. Li, J. Sculley and H.-C. Zhou, *Chem. Rev.*, 2012, **112**, 869–932.
32 J.-R. Li, Y. Ma, M. C. McCarthy, J. Sculley, J. Yu, H.-K. Jeong, P. B. Balbuena and H.-C. Zhou, *Coord. Chem. Rev.*, 2011, **255**, 1791–1823.
33 B. Van de Voorde, B. Bueken, J. Denayer and D. De Vos, *Chem. Soc. Rev.*, 2014, **43**, 5766–5788.
34 M. S. Denny, J. C. Moreton, L. Benz and S. M. Cohen, *Nat. Rev. Mater.*, 2016, **1**, 16078.
35 D. Banerjee, C. M. Simon, A. M. Plonka, R. K. Motkuri, J. Liu, X. Chen, B. Smit, J. B. Parise, M. Haranczyk and P. K. Thallapally, *Nat. Commun.*, 2016, **7**, ncomms11831.
36 Q. Gao, J. Xu and X.-H. Bu, *Coord. Chem. Rev.*, 2019, **378**, 17–31.
37 Z. R. Herm, E. D. Bloch and J. R. Long, *Chem. Mater.*, 2014, **26**, 323–338.
38 E. D. Bloch, W. L. Queen, R. Krishna, J. M. Zadrozny, C. M. Brown and J. R. Long, *Science*, 2012, **335**, 1606.
39 Z. Bao, G. Chang, H. Xing, R. Krishna, Q. Ren and B. Chen, *Energy Environ. Sci.*, 2016, **9**, 3612–3641.
40 K.-J. Chen, D. G. Madden, S. Mukherjee, T. Pham, K. A. Forrest, A. Kumar, B. Space, J. Kong, Q.-Y. Zhang and M. J. Zaworotko, *Science*, 2019, **366**, 241.
41 X. Cui, K. Chen, H. Xing, Q. Yang, R. Krishna, Z. Bao, H. Wu, W. Zhou, X. Dong, Y. Han, B. Li, Q. Ren, M. J. Zaworotko and B. Chen, *Science*, 2016, **353**, 141.
42 Y.-L. Peng, T. Pham, P. Li, T. Wang, Y. Chen, K.-J. Chen, K. A. Forrest, B. Space, P. Cheng, M. J. Zaworotko and Z. Zhang, *Angew. Chem., Int. Ed.*, 2018, **57**, 10971–10975.
43 O. M. Yaghi, *ACS Cent. Sci.*, 2019, **5**, 1295–1300.
44 X. Feng, X. Ding and D. Jiang, *Chem. Soc. Rev.*, 2012, **41**, 6010–6022.
45 P. J. Waller, F. Gándara and O. M. Yaghi, *Acc. Chem. Res.*, 2015, **48**, 3053–3063.
46 C. S. Diercks and O. M. Yaghi, *Science*, 2017, **355**, eaal1585.
47 S. S. Han, J. L. Mendoza-Cortés and W. A. Goddard III, *Chem. Soc. Rev.*, 2009, **38**, 1460–1476.
48 S.-Y. Ding and W. Wang, *Chem. Soc. Rev.*, 2013, **42**, 548–568.
49 N. Huang, P. Wang and D. Jiang, *Nat. Rev. Mater.*, 2016, **1**, 16068.
50 S. M. J. Rogge, A. Bavykina, J. Hajek, H. Garcia, A. I. Olivos-Suarez, A. Sepúlveda-Escribano, A. Vimont, G. Clet, P. Bazin, F. Kapteijn, M. Daturi, E. V. Ramos-Fernandez, F. X. Llabrés i Xamena, V. Van Speybroeck and J. Gascon, *Chem. Soc. Rev.*, 2017, **46**, 3134–3184.
51 M. Mastalerz, *Angew. Chem., Int. Ed.*, 2008, **47**, 445–447.
52 J. L. Segura, M. J. Mancheño and F. Zamora, *Chem. Soc. Rev.*, 2016, **45**, 5635–5671.
53 R. P. Bisbey and W. R. Dichtel, *ACS Cent. Sci.*, 2017, **3**, 533–543.
54 U. Díaz and A. Corma, *Coord. Chem. Rev.*, 2016, **311**, 85–124.
55 F. Beuerle and B. Gole, *Angew. Chem., Int. Ed.*, 2018, **57**, 4850–4878.
56 B. J. Smith, L. R. Parent, A. C. Overholts, P. A. Beaucage, R. P. Bisbey, A. D. Chavez, N. Hwang, C. Park, A. M. Evans, N. C. Gianneschi and W. R. Dichtel, *ACS Cent. Sci.*, 2017, **3**, 58–65.
57 D. Jiang, X. Chen, K. Geng, R. Liu, K. T. Tan, Y. Gong, Z. Li, S. Tao and Q. Jiang, *Angew. Chem., Int. Ed.*, 2019, **58**, 2–44.
58 M. S. Lohse and T. Bein, *Adv. Funct. Mater.*, 2018, **28**, 1705553.
59 Y. Song, Q. Sun, B. Aguila and S. Ma, *Adv. Sci.*, 2019, **6**, 1801410.
60 H. L. Qian, C. X. Yang, W. L. Wang, C. Yang and X. P. Yan, *J. Chromatogr. A*, 2018, **1542**, 1–18.
61 S. Yuan, X. Li, J. Zhu, G. Zhang, P. Van Puyvelde and B. Van der Bruggen, *Chem. Soc. Rev.*, 2019, **48**, 2665–2681.
62 C. Zhang, B. H. Wu, M. Q. Ma, Z. Wang and Z. K. Xu, *Chem. Soc. Rev.*, 2019, **48**, 3811–3841.
63 A. P. Côté, A. I. Benin, N. W. Ockwig, M. Keeffe, A. J. Matzger and O. M. Yaghi, *Science*, 2005, **310**, 1166.
64 A. P. Côté, H. M. El-Kaderi, H. Furukawa, J. R. Hunt and O. M. Yaghi, *J. Am. Chem. Soc.*, 2007, **129**, 12914–12915.
65 S. Wan, J. Guo, J. Kim, H. Ihee and D. Jiang, *Angew. Chem., Int. Ed.*, 2009, **48**, 5439–5442.
66 F. J. Uribe-Romo, J. R. Hunt, H. Furukawa, C. Klöck, M. O'Keeffe and O. M. Yaghi, *J. Am. Chem. Soc.*, 2009, **131**, 4570–4571.
67 F. J. Uribe-Romo, C. J. Doonan, H. Furukawa, K. Oisaki and O. M. Yaghi, *J. Am. Chem. Soc.*, 2011, **133**, 11478–11481.
68 S. Dalapati, S. Jin, J. Gao, Y. Xu, A. Nagai and D. Jiang, *J. Am. Chem. Soc.*, 2013, **135**, 17310–17313.
69 S. Wang, Q. Wang, P. Shao, Y. Han, X. Gao, L. Ma, S. Yuan, X. Ma, J. Zhou, X. Feng and B. Wang, *J. Am. Chem. Soc.*, 2017, **139**, 4258–4261.
70 M. R. Rao, Y. Fang, S. De Feyter and D. F. Perepichka, *J. Am. Chem. Soc.*, 2017, **139**, 2421–2427.

71 P. Kuhn, M. Antonietti and A. Thomas, *Angew. Chem.*, 2008, **120**, 3499–3502.
72 M. Liu, Q. Huang, S. Wang, Z. Li, B. Li, S. Jin and B. Tan, *Angew. Chem.*, 2018, **130**, 12144–12148.
73 Q. Fang, Z. Zhuang, S. Gu, R. B. Kaspar, J. Zheng, J. Wang, S. Qiu and Y. Yan, *Nat. Commun.*, 2014, **5**, 4503.
74 J. Guo, Y. Xu, S. Jin, L. Chen, T. Kaji, Y. Honsho, M. A. Addicoat, J. Kim, A. Saeki, H. Ihee, S. Seki, S. Irle, M. Hiramoto, J. Gao and D. Jiang, *Nat. Commun.*, 2013, **4**, 2736.
75 X. Zhuang, W. Zhao, F. Zhang, Y. Cao, F. Liu, S. Bi and X. Feng, *Polym. Chem.*, 2016, **7**, 4176–4181.
76 E. Jin, M. Asada, Q. Xu, S. Dalapati, M. A. Addicoat, M. A. Brady, H. Xu, T. Nakamura, T. Heine, Q. Chen and D. Jiang, *Science*, 2017, **357**, 673.
77 X. Li, Z. Wang, J. Sun, J. Gao, Y. Zhao, P. Cheng, B. Aguila, S. Ma, Y. Chen and Z. Zhang, *Chem. Commun.*, 2019, **55**, 5423–5426.
78 H. Li, Q. Pan, Y. Ma, X. Guan, M. Xue, Q. Fang, Y. Yan, V. Valtchev and S. Qiu, *J. Am. Chem. Soc.*, 2016, **138**, 14783–14788.
79 J. Zhang, X. Han, X. Wu, Y. Liu and Y. Cui, *J. Am. Chem. Soc.*, 2017, **139**, 8277–8285.
80 S.-Y. Ding, J. Gao, Q. Wang, Y. Zhang, W.-G. Song, C.-Y. Su and W. Wang, *J. Am. Chem. Soc.*, 2011, **133**, 19816–19822.
81 H. Vardhan, A. M. Al-Enizi, A. Nafady and S. Ma, *Nanoscale*, 2019, **11**, 21679–21708.
82 Q. Sun, B. Aguila and S. Ma, *Trends Chem.*, 2019, **1**, 292–303.
83 Q. Fang, J. Wang, S. Gu, R. B. Kaspar, Z. Zhuang, J. Zheng, H. Guo, S. Qiu and Y. Yan, *J. Am. Chem. Soc.*, 2015, **137**, 8352–8355.
84 G. Zhang, X. Li, Q. Liao, Y. Liu, K. Xi, W. Huang and X. Jia, *Nat. Commun.*, 2018, **9**, 2785.
85 Q. Sun, B. Aguila, J. Perman, T. Butts, F.-S. Xiao and S. Ma, *Chem*, 2018, **4**, 1726–1739.
86 A. Halder, M. Ghosh, A. Khayum M, S. Bera, M. Addicoat, H. S. Sasmal, S. Karak, S. Kurungot and R. Banerjee, *J. Am. Chem. Soc.*, 2018, **140**, 10941–10945.
87 C. R. Mulzer, L. Shen, R. P. Bisbey, J. R. McKone, N. Zhang, H. D. Abruña and W. R. Dichtel, *ACS Cent. Sci.*, 2016, **2**, 667–673.
88 H. Ma, H. Ren, S. Meng, Z. Yan, H. Zhao, F. Sun and G. Zhu, *Chem. Commun.*, 2013, **49**, 9773–9775.
89 H. Oh, S. B. Kalidindi, Y. Um, S. Bureekaew, R. Schmid, R. A. Fischer and M. Hirscher, *Angew. Chem., Int. Ed.*, 2013, **52**, 13219–13222.
90 Z. Li, X. Feng, Y. Zou, Y. Zhang, H. Xia, X. Liu and Y. Mu, *Chem. Commun.*, 2014, **50**, 13825–13828.
91 J. Fu, S. Das, G. Xing, T. Ben, V. Valtchev and S. Qiu, *J. Am. Chem. Soc.*, 2016, **138**, 7673–7680.
92 C.-X. Yang, C. Liu, Y.-M. Cao and X.-P. Yan, *Chem. Commun.*, 2015, **51**, 12254–12257.
93 K. Dey, M. Pal, K. C. Rout, S. Kunjattu H, A. Das, R. Mukherjee, U. K. Kharul and R. Banerjee, *J. Am. Chem. Soc.*, 2017, **139**, 13083–13091.
94 H.-L. Qian, C.-X. Yang and X.-P. Yan, *Nat. Commun.*, 2016, **7**, 12104.
95 L.-H. Liu, C.-X. Yang and X.-P. Yan, *J. Chromatogr. A*, 2017, **1279**, 137–144.
96 L. Jiang, Y. Tian, T. Sun, Y. Zhu, H. Ren, X. Zou, Y. Ma, K. R. Meihaus, J. R. Long and G. Zhu, *J. Am. Chem. Soc.*, 2018, **140**, 15724–15730.
97 G. Lin, H. Ding, D. Yuan, B. Wang and C. Wang, *J. Am. Chem. Soc.*, 2016, **138**, 3302–3305.
98 E. L. Spitler, B. T. Koo, J. L. Novotney, J. W. Colson, F. J. Uribe-Romo, G. D. Gutierrez, P. Clancy and W. R. Dichtel, *J. Am. Chem. Soc.*, 2011, **133**, 19416–19421.
99 Y. Zhao, K. X. Yao, B. Teng, T. Zhang and Y. Han, *Energy Environ. Sci.*, 2013, **6**, 3684–3692.
100 A. Nagai, Z. Guo, X. Feng, S. Jin, X. Chen, X. Ding and D. Jiang, *Nat. Commun.*, 2011, **2**, 536.
101 C. Gao, J. Li, S. Yin, G. Lin, T. Ma, Y. Meng, J. Sun and C. Wang, *Angew. Chem., Int. Ed.*, 2019, **58**, 9770–9775.
102 X. Wang, X. Han, J. Zhang, X. Wu, Y. Liu and Y. Cui, *J. Am. Chem. Soc.*, 2016, **138**, 12332–12335.
103 W. Cao, W. D. Wang, H.-S. Xu, I. V. Sergeyev, J. Struppe, X. Wang, F. Mentink-Vigier, Z. Gan, M.-X. Xiao, L.-Y. Wang, G.-P. Chen, S.-Y. Ding, S. Bai and W. Wang, *J. Am. Chem. Soc.*, 2018, **140**, 6969–6977.
104 H. Xu, J. Gao and D. Jiang, *Nat. Chem.*, 2015, **7**, 905–912.
105 Z. Li, H. Li, X. Guan, J. Tang, Y. Yusran, Z. Li, M. Xue, Q. Fang, Y. Yan, V. Valtchev and S. Qiu, *J. Am. Chem. Soc.*, 2017, **139**, 17771–17774.
106 N. Huang, X. Chen, R. Krishna and D. J. A. C. Jiang, *Angew. Chem., Int. Ed.*, 2015, **54**, 2986–2990.
107 N. W. Ockwig and T. M. Nenoff, *Chem. Rev.*, 2007, **107**, 4078–4110.
108 R. W. Baker, *Ind. Eng. Chem. Res.*, 2002, **41**, 1393–1411.
109 P. Bernardo, E. Drioli and G. Golemme, *Ind. Eng. Chem. Res.*, 2009, **48**, 4638–4663.
110 M. S. El-Bourawi, Z. Ding, R. Ma and M. Khayet, *J. Membr. Sci.*, 2006, **285**, 4–29.
111 B. Zornoza, C. Tellez, J. Coronas, J. Gascon and F. Kapteijn, *Microporous Mesoporous Mater.*, 2013, **166**, 67–78.
112 B. P. Biswal, H. D. Chaudhari, R. Banerjee and U. K. Kharul, *Chem. – Eur. J.*, 2016, **22**, 4695–4699.
113 G. Li, K. Zhang and T. Tsuru, *ACS Appl. Mater. Interfaces*, 2017, **9**, 8433–8436.
114 M. Shan, B. Seoane, E. Rozhko, A. Dikhtiarenko, G. Clet, F. Kapteijn and J. Gascon, *Chem. – Eur. J.*, 2016, **22**, 14467–14470.
115 Z. Kang, Y. Peng, Y. Qian, D. Yuan, M. A. Addicoat, T. Heine, Z. Hu, L. Tee, Z. Guo and D. Zhao, *Chem. Mater.*, 2016, **28**, 1277–1285.
116 H. Yang, H. Wu, F. Pan, Z. Li, H. Ding, G. Liu, Z. Jiang, P. Zhang, X. Cao and B. Wang, *J. Membr. Sci.*, 2016, **520**, 583–595.
117 H. Yang, L. Yang, H. Wang, Z. Xu, Y. Zhao, Y. Luo, N. Nasir, Y. Song, H. Wu, F. Pan and Z. Jiang, *Nat. Commun.*, 2019, **10**, 2101.

118 C. R. DeBlase, K. Hernández-Burgos, K. E. Silberstein, G. G. Rodríguez-Calero, R. P. Bisbey, H. D. Abruña and W. R. Dichtel, *ACS Nano*, 2015, **9**, 3178–3183.
119 D. D. Medina, M. L. Petrus, A. N. Jumabekov, J. T. Margraf, S. Weinberger, J. M. Rotter, T. Clark and T. Bein, *ACS Nano*, 2017, **11**, 2706–2713.
120 J. I. Feldblyum, C. H. McCreery, S. C. Andrews, T. Kurosawa, E. J. G. Santos, V. Duong, L. Fang, A. L. Ayzner and Z. Bao, *Chem. Commun.*, 2015, **51**, 13894–13897.
121 D. D. Medina, J. M. Rotter, Y. Hu, M. Dogru, V. Werner, F. Auras, J. T. Markiewicz, P. Knochel and T. Bein, *J. Am. Chem. Soc.*, 2015, **137**, 1016–1019.
122 Y. Zhao, L. Guo, F. Gándara, Y. Ma, Z. Liu, C. Zhu, H. Lyu, C. A. Trickett, E. A. Kapustin, O. Terasaki and O. M. Yaghi, *J. Am. Chem. Soc.*, 2017, **139**, 13166–13172.
123 J. W. Colson, A. R. Woll, A. Mukherjee, M. P. Levendorf, E. L. Spitler, V. B. Shields, M. G. Spencer, J. Park and W. R. Dichtel, *Science*, 2011, **332**, 228.
124 H. Fan, A. Mundstock, J. Gu, H. Meng and J. Caro, *J. Mater. Chem. A*, 2018, **6**, 16849–16853.
125 S. Das and T. Ben, *Dalton Trans.*, 2018, **47**, 7206–7212.
126 M. Matsumoto, L. Valentino, G. M. Stiehl, H. B. Balch, A. R. Corcos, F. Wang, D. C. Ralph, B. J. Mariñas and W. R. Dichtel, *Chem*, 2018, **4**, 308–317.
127 P. Shao, J. Li, F. Chen, L. Ma, Q. Li, M. Zhang, J. Zhou, A. Yin, X. Feng and B. Wang, *Angew. Chem.*, 2018, **130**, 16739–16743.
128 S. Kandambeth, B. P. Biswal, H. D. Chaudhari, K. C. Rout, H. S. Kunjattu, S. Mitra, S. Karak, A. Das, R. Mukherjee, U. K. Kharul and R. Banerjee, *Adv. Mater.*, 2017, **29**, 1603945.
129 W. Zhang, L. Zhang, H. Zhao, B. Li and H. Ma, *J. Mater. Chem. A*, 2018, **6**, 13331–13339.
130 Z. Wang, Q. Yu, Y. Huang, H. An, Y. Zhao, Y. Feng, X. Li, X. Shi, J. Liang, F. Pan, P. Cheng, Y. Chen, S. Ma and Z. Zhang, *ACS Cent. Sci.*, 2019, **5**, 1352–1359.
131 M. Zhang, L. Li, Q. Lin, M. Tang, Y. Wu and C. Ke, *J. Am. Chem. Soc.*, 2019, **141**, 5154–5158.
132 R. S. Haszeldine, *Science*, 2009, **325**, 1644.
133 A. A. Olajire, *Energy*, 2010, **35**, 2610–2628.
134 M. R. Raupach, G. Marland, P. Ciais, C. Le Quéré, J. G. Canadell, G. Klepper and C. B. Field, *Proc. Natl. Acad. Sci. U. S. A.*, 2007, **104**, 10288.
135 Y. Zeng, R. Zou and Y. Zhao, *Adv. Mater.*, 2016, **28**, 2855–2873.
136 G. T. J. S. Rochelle, *Science*, 2009, **325**, 1652–1654.
137 M.-M. Titirici, R. J. White, N. Brun, V. L. Budarin, D. S. Su, F. del Monte, J. H. Clark and M. J. MacLachlan, *Chem. Soc. Rev.*, 2015, **44**, 250–290.
138 J. Wang, L. Huang, R. Yang, Z. Zhang, J. Wu, Y. Gao, Q. Wang, D. O'Hareb and Z. Zhong, *Energy Environ. Sci.*, 2014, **7**, 3478–3518.
139 A. A. Olajire, *J. CO2 Util.*, 2017, **17**, 137–161.
140 Y. Ding, Y. Wang, Y. Su, Z. Yang, J. Liu, X. Hua and H. L. Wei, *Chin. Chem. Lett.*, 2020, **31**, 193–196.
141 S. Zhao, B. Dong, R. Ge, C. Wang, X. Song, W. Ma, Y. Wang, C. Hao, X. Guo and Y. Gao, *RSC Adv.*, 2016, **6**, 38774–38781.
142 S. Dey, A. Bhunia, H. Breitzke, P. B. Groszewicz, G. Buntkowsky and C. Janiak, *J. Mater. Chem. A*, 2017, **5**, 3609–3620.
143 S. Kandambeth, A. Mallick, B. Lukose, M. V. Mane, T. Heine and R. Banerjee, *J. Am. Chem. Soc.*, 2012, **134**, 19524–19527.
144 H. Wei, S. Chai, N. Hu, Z. Yang, L. Wei and L. Wang, *Chem. Commun.*, 2015, **51**, 12178–12181.
145 D. B. Shinde, M. Ostwal, X. Wang, A. M. Hengne, Y. Liu, G. Sheng, K.-W. Huang and Z. Lai, *CrystEngComm*, 2018, **20**, 7621–7625.
146 Q. Gao, L. Bai, X. Zhang, P. Wang, P. Li, Y. Zeng, R. Zou and Y. Zhao, *Chin. J. Chem.*, 2015, **33**, 90–94.
147 Z. Kahveci, T. Lslamoglu, G. A. Shar, R. S. Ding and H. M. EI-Kaderi, *CrystEngComm*, 2013, **15**, 1524–1527.
148 G. Rabbani, A. K. Sekizkardes, Z. Kahveci, T. E. Reich, R. S. Ding and H. M. EI-Kaderi, *Chem. – Eur. J.*, 2013, **19**, 3324–3328.
149 H. Furukawa and O. M. Yaghi, *J. Am. Chem. Soc.*, 2009, **131**, 8875–8883.
150 Z. Li, Y. Zhi, X. Feng, X. Ding, Y. Zou, X. Liu and Y. Mu, *Chem. – Eur. J.*, 2015, **21**, 12079–12084.
151 Q. Chen, M. Luo, P. Hammershoj, D. Zhou, Y. Han, B. W. Laursen, C. G. Yan and B. H. Han, *J. Am. Chem. Soc.*, 2012, **134**, 6084–6087.
152 Y. Zhu, H. Long and W. Zhang, *Chem. Mater.*, 2013, **25**, 1630–1635.
153 P. Arab, M. G. Rabbani, A. K. Sekizkardes, T. Islamoglu and H. M. El-Kaderi, *Chem. Mater.*, 2014, **26**, 1385–1392.
154 R. Ge, D. Hao, Q. Shi, B. Dong, W. Leng, C. Wang and Y. Gao, *J. Chem. Eng. Data*, 2016, **61**, 1904–1909.
155 N. Huang, R. Krishna and D. Jiang, *J. Am. Chem. Soc.*, 2015, **137**, 7079–7082.
156 A. Sharma, A. Malani, N. V. Medhekar and R. Babarao, *CrystEngComm*, 2017, **19**, 6950–6963.
157 T. Yan, Y. Lan, M. Tong and C. Zhong, *ACS Sustainable Chem. Eng.*, 2019, **7**, 1220–1227.
158 X. Wu, Z. Tian, S. Wang, D. Peng, L. Yang, Y. Wu, Q. Xin, H. Wu and Z. Jiang, *J. Membr. Sci.*, 2017, **528**, 273–283.
159 M. Tong, Q. Yang, Q. Ma, D. Liu and C. Zhong, *J. Mater. Chem. A*, 2016, **4**, 124–131.
160 C. Zou, Q. Li, Y. Hua, B. Zhou, J. Duan and W. Jin, *ACS Appl. Mater. Interfaces*, 2017, **9**, 29093–29100.
161 X. Guan, Y. Ma, H. Li, Y. Yusran, M. Xue, Q. Fang, Y. Yan, V. Valtchev and S. Qiu, *J. Am. Chem. Soc.*, 2018, **140**, 4494–4498.
162 D. Lozano-Castelló, J. Alcañiz-Monge, M. A. de la Casa-Lillo, D. Cazorla-Amorós and A. Linares-Solano, *Fuel*, 2002, **81**, 1777–1803.
163 J. A. Mason, M. Veenstra and J. R. Long, *Chem. Sci.*, 2014, **5**, 32–51.
164 M. E. Casco, M. Martínez-Escandell, E. Gadea-Ramos, K. Kaneko, J. Silvestre-Albero and F. Rodríguez-Reinoso, *Chem. Mater.*, 2015, **27**, 959–964.
165 J. L. Mendoza-Cortes, T. A. Pascal and W. A. Goddard, *J. Phys. Chem. A*, 2011, **115**, 13852–13857.
166 A. Sharma, R. Babarao, N. V. Medhekar and A. Malani, *Ind. Eng. Chem. Res.*, 2018, **57**, 4767–4778.
167 J. M. Vicent-Luna, A. Luna-Triguero and S. Calero, *J. Phys. Chem. C*, 2016, **120**, 23756–23762.

168 S. B. Alahakoon, C. M. Thompson, A. X. Nguyen, G. Occhialini, G. T. McCandless and R. A. Smaldone, *Chem. Commun.*, 2016, **52**, 2843–2845.
169 C. Krishnaraj, H. S. Jena, K. Leus, H. M. Freeman, L. G. Benning and P. Van Der Voort, *J. Mater. Chem. A*, 2019, **7**, 13188–13196.
170 Y. He, Z. Zhang, S. Xiang, H. Wu, F. R. Fronczek, W. Zhou, R. Krishna, M. O'Keeffe and B. Chen, *Chem. – Eur. J.*, 2012, **18**, 1901–1904.
171 Y. He, Z. Zhang, S. Xiang, F. R. Fronczek, R. Krishna and B. Chen, *Chem. Commun.*, 2012, **48**, 6493–6495.
172 J. Duan, M. Higuchi, S. Horike, M. L. Foo, K. P. Rao, Y. Inubushi, T. Fukushima and S. Kitagawa, *Adv. Funct. Mater.*, 2013, **23**, 3525–3530.
173 A. P. Katsoulidis and M. G. Kanatzidis, *Chem. Mater.*, 2012, **24**, 471–479.
174 J. Dong, Y. Wang, G. Liu, Y. Cheng and D. Zhao, *CrystEngComm*, 2017, **19**, 4899–4904.
175 L. Li, R.-B. Lin, R. Krishna, X. Q. Wang, B. Li, H. Wu, J. P. Li, W. Zhou and B. Chen, *J. Mater. Chem. A*, 2017, **5**, 18984–18988.
176 S. Yang, A. J. Ramirez-Cuesta, R. Newby, V. Garcia-Sakai, P. Manuel, S. K. Callear, S. I. Campbell, C. C. Tang and M. Schröder, *Nat. Chem.*, 2014, **7**, 121–129.
177 A. Hazra, S. Jana, S. Bonakala, S. Balasubramanian and T. K. Maji, *Chem. Commun.*, 2017, **53**, 4907–4910.
178 Y. Tao, R. Krishna, L. X. Yang, Y. L. Fan, L. Wang, Z. Gao, J. B. Xiong, L. J. Sun and F. Luo, *Inorg. Chem. Front.*, 2019, **6**, 2921–2926.
179 Y. Lu, J. He, Y. Chen, H. Wang, Y. Zhao, Y. Han and Y. Ding, *Macromol. Rapid Commun.*, 2018, **39**, 1700468.
180 L. Jiang, P. Wang, M. Li, P. Zhang, J. Li, J. Liu, Y. Ma, H. Ren and G. Zhu, *Chem. – Eur. J.*, 2019, **25**, 9045–9051.
181 J. A. Turner, *Science*, 2004, **305**, 972.
182 N. Hallale and F. Liu, *Adv. Environ. Res.*, 2001, **6**, 81–98.
183 H. Lin, E. Van Wagner, B. D. Freeman, L. G. Toy and R. P. Gupta, *Science*, 2006, **311**, 639.
184 Z. R. Herm, J. A. Swisher, B. Smit, R. Krishna and J. R. Long, *J. Am. Chem. Soc.*, 2011, **133**, 5664–5667.
185 M. Hong, S. Li, J. L. Falconer and R. D. Noble, *J. Membr. Sci.*, 2008, **307**, 277–283.
186 Y. Li, Z. Zhou, P. Shen and Z. Chen, *Chem. Commun.*, 2010, **46**, 3672–3674.
187 Y. Liu, D. Liu, Q. Yang, C. Zhong and J. Mi, *Ind. Eng. Chem. Res.*, 2010, **49**, 2902–2906.
188 Y. Wang, J. Li, Q. Yang and C. Zhong, *ACS Appl. Mater. Interfaces*, 2016, **8**, 8694–8701.
189 S. S. Han, H. Furukawa, O. M. Yaghi and W. A. Goddard, *J. Am. Chem. Soc.*, 2008, **130**, 11580–11581.
190 D. Cao, J. Lan, W. Wang and B. Smit, *Angew. Chem., Int. Ed.*, 2009, **48**, 4730–4733.
191 W. Salim and W. S. W. Ho, *Curr. Opin. Chem. Eng.*, 2018, **21**, 96–102.
192 Z. Xiang, D. Cao, W. Wang, W. Yang, B. Han and J. Lu, *J. Phys. Chem. C*, 2012, **116**, 5974–5980.
193 H. Lu, C. Wang, J. Chen, R. Ge, W. Leng, B. Dong, J. Huang and Y. Gao, *Chem. Commun.*, 2015, **51**, 15562–15565.
194 H. Fan, A. Mundstock, A. Feldhoff, A. Knebel, J. Gu, H. Meng and J. Caro, *J. Am. Chem. Soc.*, 2018, **140**, 10094–10098.
195 F. Keppler, J. T. G. Hamilton, W. C. McRoberts, I. Vigano, M. Braß and T. Rockmann, *New Phytol.*, 2008, **178**, 808–814.
196 H. K. Rae, *Separation of Hydrogen Isotopes*, American Chemical Society, Washington DC, 1978, pp. 1–26.
197 J. J. M. Beenakker, V. D. Borman and S. Y. Krylov, *Chem. Phys. Lett.*, 1995, **232**, 379–382.
198 A. Schneemann, V. Bon, I. Schwedler, I. Senkovska, S. Kaskel and R. A. Fischer, *Chem. Soc. Rev.*, 2014, **43**, 6062–6096.
199 S. Horike, S. Shmomura and S. Kitagawa, *Nat. Chem.*, 2009, **23**, 695.
200 F. J. Uribe-Romo, J. R. Hunt, H. Furukawa, C. Klock, M. O'Keeffe and O. M. Yaghi, *J. Am. Chem. Soc.*, 2009, **131**, 4570–4571.
201 T. Ma, J. Li, J. Niu, L. Zhang, A. S. Etman, C. Lin, D. Shi, P. Chen, L.-H. Li, X. Du, J. Sun and W. Wang, *J. Am. Chem. Soc.*, 2018, **140**, 6763–6766.
202 T. Ma, E. A. Kapustin, S. X. Yin, L. Liang, Z. Zhou, J. Niu, L.-H. Li, Y. Wang, J. Su, J. Li, X. Wang, W. D. Wang, W. Wang, J. Sun and O. M. Yaghi, *Science*, 2018, **361**, 48–52.
203 E. Feitelson and J. Chenoweth, *Water Policy*, 2002, **4**, 263–281.
204 M. Elimelech and W. A. Phillip, *Science*, 2011, **333**, 712–717.
205 H. Zhou and D. W. Smith, *J. Environ. Eng. Sci.*, 2002, **1**, 247–264.
206 V. K. Gupta, I. Ali, T. A. Saleh, A. Nayak and S. Agarwal, *RSC Adv.*, 2012, **2**, 6380–6388.
207 G.-H. Ning, Z. Chen, Q. Gao, W. Tang, Z. Chen, C. Liu, B. Tian, X. Li and K. P. Loh, *J. Am. Chem. Soc.*, 2017, **139**, 8897–8904.
208 S. S. Ray, S.-S. Chen, C.-W. Li, N. C. Nguyen and H. T. Nguyen, *RSC Adv.*, 2016, **6**, 85495–85514.
209 X. Li, Y. Liu, J. Wang, J. Gascon, J. Li and B. V. D. Bruggen, *Chem. Soc. Rev.*, 2017, **46**, 7124–7144.
210 M. Matsumoto, L. Valentino, G. M. Stiehl, H. B. Balch, A. R. Corcos, F. Wang, D. C. Ralph, B. J. Mariñas and W. R. Dichtel, *Chem*, 2017, **4**, 1–10.
211 D. B. Shinde, G. Sheng, X. Li, M. Ostwal, A.-H. Emwas, K.-W. Huang and Z. Lai, *J. Am. Chem. Soc.*, 2018, **140**, 14342–14349.
212 R. Wang, X. Shi, A. Xiao, W. Zhou and Y. Wang, *J. Membr. Sci.*, 2018, **566**, 197–204.
213 H. Fan, J. Gu, H. Meng, A. Knebel and J. Caro, *Angew. Chem., Int. Ed.*, 2018, **57**, 4083–4087.
214 W. Zhang, L. Zhang, H. Zhao, B. Li and H. Ma, *J. Mater. Chem. A*, 2018, **6**, 13331–13339.
215 I. Gadwal, G. Sheng, R. L. Thankamony, Y. Liu, H. Li and Z. Lai, *ACS Appl. Mater. Interfaces*, 2018, **10**, 12295–12299.
216 X. Zhang, H. Li, J. Wang, D. Peng, J. Liu and Y. Zhang, *J. Membr. Sci.*, 2019, **581**, 321–330.
217 D. Li and H. Wang, *J. Mater. Chem.*, 2010, **20**, 4551–4566.
218 N. Voutchkov, *Desalination*, 2018, **431**, 2–14.
219 D. Zhou, L. Zhu, Y. Fu, M. Zhu and L. Xue, *Desalination*, 2015, **376**, 109–116.

220 K. P. Lee, T. C. Arnot and D. Mattia, *J. Membr. Sci.*, 2011, **370**, 1–22.
221 K. Zhang, Z. He, K. M. Gupta and J. Jiang, *Environ. Sci.: Water Res. Technol.*, 2017, **3**, 735–743.
222 W. Zhou, M. Wei, X. Zhang, F. Xu and Y. Wang, *ACS Appl. Mater. Interfaces*, 2019, **11**, 16847–16854.
223 V. A. Kuehl, J. Yin, P. H. H. Duong, B. Mastorovich, B. Newell, K. D. Li-Oakey, B. A. Parkinson and J. O. Hoberg, *J. Am. Chem. Soc.*, 2018, **140**, 18200–18207.
224 S.-Y. Ding, M. Dong, Y.-W. Wang, Y.-T. Chen, H.-Z. Wang, C.-Y. Su and W. Wang, *J. Am. Chem. Soc.*, 2016, **138**, 3031–3037.
225 N. Huang, L. Zhai, H. Xu and D. Jiang, *J. Am. Chem. Soc.*, 2017, **139**, 2428–2434.
226 K.-K. Yee, N. Reimer, J. Liu, S.-Y. Cheng, S.-M. Yiu, J. Weber, N. Stock and Z. Xu, *J. Am. Chem. Soc.*, 2013, **135**, 7795–7798.
227 Y. Shin, G. E. Fryxell, W. Um, K. Parker, S. V. Mattigod and R. Skaggs, *Adv. Funct. Mater.*, 2007, **17**, 2897–2901.
228 J. Liu, X. Feng, G. E. Fryxell, L.-Q. Wang, A. Y. Kim and M. Gong, *Adv. Mater.*, 1998, **10**, 161–165.
229 S. Bag, P. N. Trikalitis, P. J. Chupas, G. S. Armatas and M. G. Kanatzidis, *Science*, 2007, **317**, 490–493.
230 Q. Sun, B. Aguila, J. Perman, L. D. Earl, C. W. Abney, Y. Cheng, H. Wei, N. Nguyen, L. Wojtas and S. Ma, *J. Am. Chem. Soc.*, 2017, **139**, 2786–2793.
231 Q. Sun, B. Aguila, L. D. Earl, C. W. Abney, L. Wojtas, P. K. Thallapally and S. Ma, *Adv. Mater.*, 2018, **30**, 1705479.
232 H.-J. Da, C.-X. Yang and X.-P. Yan, *Environ. Sci. Technol.*, 2019, **53**, 5212–5220.
233 F. T. Mattrey, A. A. Makarov, E. L. Regalado, F. Bernardoni, M. Figus, M. B. Hicks, J. Zheng, L. Wang, W. Schafer, V. Antonucci, S. E. Hamilton, K. Zawatzky and C. J. Welch, *TrAC, Trends Anal. Chem.*, 2017, **95**, 36–46.
234 C. Wu, P. Xu, X. Wang, D. Shou, N. Wang and Y. Zhu, *Anal. Methods*, 2019, **11**, 3590–3596.
235 K. M. Muhammad Ismayil, O. Manaf, A. Sujith and R. Antony, *Mater. Lett.*, 2019, **252**, 321–324.
236 A. Speltini, D. Merli and A. Profumo, *Anal. Chim. Acta*, 2013, **783**, 1–16.
237 J. Zhang and Z. Chen, *J. Chromatogr. A*, 2017, **1530**, 1–18.
238 K. Hu, W. Zhang, H. Yang, Y. Cui, J. Zhang, W. Zhao, A. Yu and S. Zhang, *Talanta*, 2016, **152**, 392–400.
239 C. Lu, S. Liu, J. Xu, Y. Ding and G. Ouyang, *Anal. Chim. Acta*, 2016, **902**, 205–211.
240 K. Tanaka, T. Muraoka, Y. Otubo, H. Takahashi and A. Ohnishi, *RSC Adv.*, 2016, **6**, 21293–21301.
241 X. Niu, S. Ding, W. Wang, Y. Xu, Y. Xu, H. Chen and X. Chen, *J. Chromatogr. A*, 2016, **1436**, 109–117.
242 T. Bao, P. Tang, D. Kong, Z. Mao and Z. Chen, *J. Chromatogr. A*, 2016, **1445**, 140–148.
243 D. Kong, T. Bao and Z. Chen, *Microchim. Acta*, 2017, **184**, 1169–1176.
244 D. Kong and Z. Chen, *Electrophoresis*, 2018, **39**, 2912–2918.
245 N. Ye, X. Wang, Q. Liu and X. Hu, *Anal. Chim. Acta*, 2018, **1028**, 113–120.
246 L.-L. Wang, C.-X. Yang and X.-P. Yan, *ChemPlusChem*, 2017, **82**, 933–938.
247 K. Zhang, S.-L. Cai, Y.-L. Yan, Z.-H. He, H.-M. Lin, X.-L. Huang, S.-R. Zheng, J. Fan and W.-G. Zhang, *J. Chromatogr. A*, 2017, **1519**, 100–109.
248 W. Zhao, K. Hu, C. Hu, X. Wang, A. Yu and S. Zhang, *J. Chromatogr. A*, 2017, **1487**, 83–88.
249 L. Chen, J. Gao, Q. Wu, H. Li, S. Dong, X. Shi and L. Zhao, *Eur. Polym. J.*, 2019, **116**, 9–19.
250 J. Huang, X. Han, S. Yang, Y. Cao, C. Yuan, Y. Liu, J. Wang and Y. Cui, *J. Am. Chem. Soc.*, 2019, **141**, 8996–9003.
251 R. Sancho and C. Minguillón, *Chem. Soc. Rev.*, 2009, **38**, 797–805.
252 J. M. Alex, V. Corvaglia, X. Hu, S. Engilberge, I. Huc and P. B. Crowley, *Chem. Commun.*, 2019, **55**, 11087–11090.
253 V. Nosek and J. Míšek, *Chem. Commun.*, 2019, **55**, 10480–10483.
254 R. E. Morris and X. Bu, *Nat. Chem.*, 2010, **2**, 353–361.
255 Y. Peng, T. Gong, K. Zhang, X. Lin, Y. Liu, J. Jiang and Y. Cui, *Nat. Commun.*, 2014, **5**, 4406.
256 W. Xuan, C. Ye, M. Zhang, Z. Chen and Y. Cui, *Chem. Sci.*, 2013, **4**, 3154–3159.
257 H.-L. Qian, C.-X. Yang and X.-P. Yan, *Nat. Commun.*, 2016, **7**, 12104.
258 X. Han, J. Huang, C. Yuan, Y. Liu and Y. Cui, *J. Am. Chem. Soc.*, 2018, **140**, 892–895.
259 S. Zhang, Y. Zheng, H. An, B. Aguila, C.-X. Yang, Y. Dong, W. Xie, P. Cheng, Z. Zhang, Y. Chen and S. Ma, *Angew. Chem., Int. Ed.*, 2018, **57**, 16754–16759.
260 G. Lin, H. Ding, R. Chen, Z. Peng, B. Wang and C. Wang, *J. Am. Chem. Soc.*, 2017, **139**, 8705–8709.